8-1-2003

Fatigue Resistance of Corrugated Web Girders

Richard Sause

Hassam H. Abbas

Robert G. Driver

Kengo Anami

John W. Fisher

Fatigue Resistance of Corrugated Web Girders

Work Area 3
Pennsylvania Innovative High Performance Steel
Bridge Demonstration Project

Report to
Commonwealth of Pennsylvania
Department of Transportation
Contract No. 359810

by

Richard Sause, Hassan H. Abbas, Robert G. Driver,
Kengo Anami, and John W. Fisher

ATLSS Report No. 03-20

August 2003

ATLSS is a National Center for Engineering Research
on Advanced Technology for Large Structural Systems

117 ATLSS Drive
Bethlehem, PA 18015-4729

Phone: (610)758-3525
Fax: (610)758-5902

www.atlss.lehigh.edu
Email: inatl@lehigh.edu

Technical Report Documentation Page

1. Report No.	2. Government Accession No.	3. Recipient's Catalog No.
FHWA-PA-2004-005-98-10 (c)		

4. Title and Subtitle	5. Report Date
Fatigue Resistance of Corrugated Web Girders: Work Area 3, Pennsylvania Innovative High Performance Steel Bridge Demonstration Project	August 2003
	6. Performing Organization Code 4D371 (CAGE)

7. Author(s)	8. Performing Organization Report No.
Richard Sause, Hassan H. Abbas, Robert G. Driver, Kengo Anami, and John W. Fisher	ATLSS Report No. 03-20

9. Performing Organization Name and Address	10. Work Unit No. (TRAIS)
Advanced Technology for Large Structural Systems (ATLSS) Center Lehigh University 117 ATLSS Drive Bethlehem PA 18015-4729	**11. Contract or Grant No.** 359810

12. Sponsoring Agency Name and Address	13. Type of Report and Period Covered
The Pennsylvania Department of Transportation Bureau of Planning and Research Commonwealth Keystone Building 400 North Street, 6th Floor Harrisburg, PA 17120-0064	Final Report
	14. Sponsoring Agency Code

15. Supplementary Notes
COTR: Thomas P. Macioce

See Report Nos.: FHWA-PA-2004-005-98-10 (a), (b), (d), and (e) for related work.

16. Abstract
The Pennsylvania Department of Transportation (PennDOT) has proposed to design and construct a high performance steel demonstration bridge using HPS-485W (HPS-70W) steel in combination with I-shaped girders with corrugated webs. Toward this goal, a coordinated program of design and fabrication studies, and applied laboratory research (testing and analysis) has been conducted to develop details and design criteria for the bridge. This program, titled the "Pennsylvania High Performance Steel Bridge Demonstration Project", consisted of the following Work Areas: (1) corrugated web girder corrugation shape and strength criteria; (2) corrugated web girder fabrication; (3) fatigue resistance of corrugated web girders; (4) corrugated web girder field splices; and (5) diaphragms with flange rotational restraint braces. This report addresses Work Area 3, fatigue resistance of corrugated web girders.

The report describes work conducted to provide fatigue strength data representative of corrugated web bridge I-girders with trapezoidal corrugations, and to propose fatigue design criteria for corrugated web I-girders for bridges. Eight fatigue tests on large-scale girder specimens with full-scale trapezoidal webs were conducted. The test specimens were made from ASTM A709 HPS-485W (HPS-70W) steel using gas metal arc welding (GMAW) for the web-to-flange fillet welds. The fatigue test results are reported, analyzed, and compared with results of previous research. Design criteria are recommended.

17. Key Words	18. Distribution Statement
Steel bridge, steel bridge girder, steel bridge girder fatigue, corrugated web, corrugated web girder, corrugated web girder fatigue strength, corrugated web girder fatigue resistance, high performance steel	No restrictions. This document is available from the National Technical Information Service, Springfield, VA 22161 or by request to the PennDOT Research Program.

19. Security Classif. (of this report)	20. Security Classif. (of this page)	21. No. of Pages	22. Price
Unclassified	Unclassified	51	

Fatigue Resistance of Corrugated Web Girders

Work Area 3
Pennsylvania Innovative High Performance Steel
Bridge Demonstration Project

Report to
Commonwealth of Pennsylvania
Department of Transportation
Contract No. 359810

by

Richard Sause, Ph.D.
Professor of Structural Engineering
Lehigh University

Hassan H. Abbas, Ph.D.
Formerly, Graduate Research Assistant
Lehigh University

Robert G. Driver, Ph.D.
Associate Professor of Civil Engineering
University of Alberta

Kengo Anami, Ph.D.
Research Associate
Lehigh University

John W. Fisher, Ph.D.
Professor Emeritus of Civil Engineering
Lehigh University

ATLSS Report No. 03-20

August 2003

ATLSS is a National Center for Engineering Research
on Advanced Technology for Large Structural Systems

117 ATLSS Drive
Bethlehem, PA 18015-4729

Phone: (610)758-3525
Fax: (610)758-5902

www.atlss.lehigh.edu
Email: inatl@lehigh.edu

Acknowledgements

This work was sponsored by the Pennsylvania Department of Transportation. Support was also provided by the Federal Highway Administration and the Pennsylvania Infrastructure Technology Alliance (funded by a grant from Pennsylvania Department of Community and Economic Development).

The Pennsylvania High Performance Steel Bridge Demonstration Project is a partnership of the ATLSS Center at Lehigh University with Drexel University (M. Elgaaly), High Steel Structures, Inc. (S. Kopp, R. Kase), and Modjeski and Masters, Inc. (W. Wassef), and involves many individuals (the primary contacts are given in parentheses). This report addresses Work Area 3 of this project. The contributions of Dr. W. Wassef of Modjeski and Masters, Inc., Dr. M. Elgaaly of Drexel University, and S. Kopp and R. Kase of High Steel Structures, Inc. to the planning stages of Work Area 3 are acknowledged. The corrugated web girder test specimens used in Work Area 3 were fabricated by High Steel Structures, Inc. The authors are grateful for the input and support of Tom Macioce, Bob Horwhat, Dave Wilhelm, and Joe Bracken from the Pennsylvania Department of Transportation. Dr. E. Kaufmann and Dr. A. Pense, from the ATLSS Center, provided valuable input on welding processes and fracture toughness considerations for corrugated web girders. Finally, the authors are grateful for the contributions of D. Yu and T. Clarke, and the contributions of the technical staff of the ATLSS Center and Fritz Engineering Lab.

The contents of this report reflect the views of the authors, who are responsible for the facts and accuracy of the data presented herein. The contents do not necessarily reflect the official views or policies of the Commonwealth of Pennsylvania at the time of publication. This report does not constitute a standard, specification or regulation.

Table of Contents

List of Tables

List of Figures

List of Figures (continued)

Abstract

The Pennsylvania Department of Transportation (PennDOT) has proposed to design and construct a high performance steel demonstration bridge using HPS-485W (HPS-70W) steel in combination with I-shaped girders with corrugated webs. To assist PennDOT, a coordinated program of design and fabrication studies, and applied laboratory research (testing and analysis) has been conducted to develop details and design criteria for the bridge. This project, titled the "Pennsylvania High Performance Steel Bridge Demonstration Project", is being conducted by the following team: (1) the ATLSS Center at Lehigh University, (2) Modjeski and Masters, Inc., (3) High Steel Structures, Inc., and (4) Drexel University. The program consists of the following Work Areas: (1) corrugated web girder corrugation shape and strength criteria; (2) corrugated web girder fabrication; (3) fatigue resistance of corrugated web girders; (4) corrugated web girder field splices; and (5) precast deck and diaphragms with flange rotational restraint braces. This report addresses Work Area 3, fatigue resistance of corrugated web girders.

The report describes work conducted to provide fatigue strength data representative of corrugated web bridge I-girders with trapezoidal corrugations, and to propose fatigue design criteria for corrugated web I-girders for bridges. Eight fatigue tests on large-scale girder specimens with full-scale trapezoidal webs were conducted. The test specimens were made from ASTM A709 HPS-485W (HPS-70W) steel using gas metal arc welding (GMAW) for the web-to-flange fillet welds. The fatigue test results are reported, analyzed, and compared with results of previous research. Design criteria are recommended.

1. Introduction

The Pennsylvania Department of Transportation (PennDOT) has proposed to design and construct a HPS demonstration bridge using HPS-485W (HPS-70W) steel in combination with innovative bridge design concepts. The site of the bridge is to be determined. The demonstration bridge will be a multiple steel I-girder bridge. The girders will be fabricated with corrugated webs, and may be braced with cross-frames that include compression flange rotational restraint braces. Precast high-performance concrete panels may be used to construct the deck without extensive use of field-placed concrete. To assist PennDOT with the development of the demonstration bridge, a coordinated program of design and fabrication studies, and applied laboratory research (testing and analysis) has been conducted to develop details and design criteria for the bridge. This project, titled the "Pennsylvania High Performance Steel (HPS) Bridge Demonstration Project", is being conducted by a team composed of the following participants: (1) the ATLSS Center at Lehigh University, (2) Modjeski and Masters, Inc., (3) High Steel Structures, Inc., and (4) Drexel University.

The coordinated program of design and fabrication studies, and applied laboratory research (testing and analysis) consists of the following work areas: (1) corrugated web girder corrugation shape and strength criteria; (2) corrugated web girder fabrication; (3) fatigue resistance of corrugated web girders; (4) corrugated web girder field splices; and (5) precast deck and diaphragms with flange rotational restraint braces. This report addresses only Work Area 3, fatigue resistance of corrugated web girders.

The objectives of this report are: (1) to provide data representative of the fatigue strength of corrugated web bridge I-girders with trapezoidal corrugations, and (2) to propose fatigue design criteria for corrugated web I-girders for bridges. To accomplish these objectives, eight fatigue tests on large-scale girder specimens with full-scale trapezoidal webs were conducted. The test specimens were made from ASTM A709 HPS-485W (HPS-70W) steel (ASTM 2001). Gas metal arc welding (GMAW) was used for the web-to-flange fillet welds. The fatigue test results are reported, analyzed, and compared with results of previous research. Design recommendations are made.

The report is organized as follows. Section 2 reviews relevant background information on fatigue design specifications and previous research on fatigue of corrugated web girders. Section 3 covers the fatigue strength tests, including the test specimens, test set-up, instrumentation, and procedure. Section 4 presents the fatigue test results, including measurements and observations, and Section 5 presents analyses of the test results and provides recommended fatigue design criteria. Section 6 provides a summary and conclusions.

2. Background

2.1. Fatigue Design Specifications

The results of the current investigation are presented in the context of the fatigue design specifications of the AASHTO LRFD bridge design specifications (AASHTO 1998). These fatigue design specifications are based primarily on work by Fisher *et al.* (1970) and Fisher *et al.* (1974), which found that the stress range and detail type are the only variables that significantly influence the fatigue strength of welded details. Other variables, such as the stress ratio, R, and yield strength, were shown to be insignificant because of the high level of residual stresses found in typical welded details.

Statistical analysis of the test data showed that for a given detail the fatigue resistance, expressed in terms of number of cycles to failure, N, is related to the stress range, σ_r, by the following logarithmic relationship:

$$\log N = \log A - B \log \sigma_r \tag{1}$$

Equation 1 has the form $y=a+bx$ and thus can be represented as a straight line. In Equation 1, $\log A$ is the $\log N$ axis intercept and B is the slope of the line as shown in Figure 1.

According to Fisher *et al.* (1970), the log transformation of Equation 1 resulted in a normal distribution of test data at nearly all levels of stress range. Consequently, a lower bound curve for design can be readily obtained from the mean curve using the standard deviation of the test data, S. For a 95% confidence limit, a lower bound design curve can be obtained by shifting the mean curve $1.96S$ along the $\log N$ axis as indicated in Figure 1. The lower bound intercept can be obtained from the mean intercept using:

$$\log A_{lower\,bound} = \log A_{mean} - 1.96S \tag{2}$$

This procedure was used to define the fatigue resistance of detail Categories A, B, C, D, and E of the AASHTO fatigue design specifications.

Keating and Fisher (1986) refined the fatigue categories of Fisher *et al*. (1970, 1974) in light of additional test results. Keating and Fisher (1986) proposed using only one slope, –3 (*i.e*., B=3), for all fatigue categories. The slopes that were previously determined, by regression analysis, were different for different categories and were close to, but not exactly, –3. In addition, Keating and Fisher (1986) defined detail Categories B′ and E′ and proposed constant amplitude fatigue limits (CAFL) for all of the fatigue detail categories. These refinements are the basis for the current AASHTO fatigue design specifications (AASHTO 1998).

Table 1 summarizes the AASHTO lower bound fatigue design curves. Note that a Category C′ with the same intercept as Category C but a different CAFL is included. The

table also provides the standard deviation for each category as reported by Keating and Fisher (1986). The standard deviations for Categories B′ and C′ were not provided by Keating and Fisher (1986), and thus it is assumed that the standard deviation for Category B′ is equal to that of Category B, and similarly the standard deviation of Category C′ is equal to that of Category C. Using the standard deviation, the mean curve for each category can be calculated from the lower bound design curve using Equation 2. The AASHTO lower bound fatigue design curves and the corresponding mean curves are plotted in Figure 2 and Figure 3, respectively.

2.2. Previous Research on Corrugated Web Girder Fatigue Strength

Previous research on the fatigue strength of corrugated web girders is summarized in this section. Harrison (1965) tested two I-girders with sinusoidal corrugations, denoted as Beam 1 and Beam 2, in 4-point bending (which produces a region of constant moment and zero shear between the load points). Figure 4(a) shows the dimensions of the web and flanges. The web-to-flange fillet welds were 6.35mm (0.25in) in size. The corrugation amplitude was 76.2mm (3in) and the corrugation wavelength was 610mm (24in) and 419mm (16.5in) for Beam 1 and Beam 2, respectively. The minimum stress applied to the tension flange was approximately 12.4MPa (1.8ksi) for both girders. The average stress range in the tension flange, based on measured strains, was 185MPa (26.9ksi) and 156MPa (22.6ksi) for Beam 1 and Beam 2, respectively. Both girders failed due to fatigue cracking.

Beam 1 failed prematurely from a notch in the flame cut edge of the flange after 1.1 million cycles. Cracking from the web-to-flange fillet weld was not reported. Thus, the reported fatigue life can be regarded as a lower bound to the fatigue life for cracks initiating at the web-to-flange fillet weld. It is important to note that the crack in Beam 1 initiated outside of the constant moment region in an area with combined bending and shear. Simple beam theory suggests that the stress range in the tension flange is lower in the shear region (where the crack initiated) than in the constant moment region. However, as discussed in detail by Abbas (2003) and summarized by Sause *et al.* (2003), flange transverse bending moments develop in corrugated web I-girders under shear force. The flange transverse bending produces transverse bending stresses that are superimposed on stresses from overall bending. The transverse bending stresses are largest at the flange tips and thus, initiation of the crack in Beam 1 at the flange tip is not surprising.

Beam 2, was tested at a lower stress range than Beam 1 and failed after 2.35 million cycles. Harrison (1965) reported that a number of fatigue cracks initiated from the web-to-flange fillet weld, one of which propagated across the flange. Although the mechanism of fatigue cracking for Beam 2 was different than that of Beam 1, failure also occurred outside of the constant moment region at a section with combined bending and shear, suggesting that flange transverse bending stresses may have made the stresses in the shear region higher than those in the constant moment region.

Korashy and Varga (1979) tested eleven girders stiffened using discrete web corrugations in 4-point bending. Figure 4(b) shows the dimensions of the web and flanges. The corrugations had a wavelength of 257mm (10.1in) and an amplitude of 78.4mm (3.09 in). The maximum inclination of the web with respect to the longitudinal axis of the girder was 45°. The web-to-flange fillet weld size was 4mm (0.16in). The stress range applied to the bottom flange varied from 132MPa (19.2ksi) to 216MPa (31.4ksi). These stresses were calculated for the top side of the bottom flange using simple beam theory. Most of the cracks initiated at the toe of the web-to-flange fillet weld where the web inclination to the longitudinal axis of the girder was at or near its maximum (*i.e,* 45°). These cracks then propagated into the flange finally leading to fracture.

Elgaaly and coworkers at Drexel University (Elgaaly *et al.* 2000, Rodriguez 2000, and Ibrahim 2001) investigated fatigue of corrugated web I-girders with trapezoidal corrugations. Rodriguez (2000) reported on tests of six girders with trapezoidal web corrugations. Figure 4(c) shows the dimensions of the web and flanges. The corrugations were 106mm (4.17in) deep with a wavelength of 500mm (19.7in). Continuous *one-sided* fillet welds were used for the web-to-flange weld. Stiffeners were provided at the load points and the reaction points to prevent web crippling. Five girders failed by fatigue cracks that initiated at or near the stiffeners. One girder failed by crack initiation from the web-to-flange fillet weld toe at a location outside of the constant moment region in an area with combined bending and shear. As explained previously, the flange stress at such a location is likely to be high due to flange transverse bending from shear. More importantly, one-sided web-to-flange fillet welds are not used in bridges, and thus, the test results from Rodriguez (2000) are not representative of corrugated web bridge girders, and are not considered further.

Ibrahim (2001) reported on tests of six girders with trapezoidal corrugations. The girders were tested in 4-point bending. Figure 4(d) shows the dimensions of the web and flanges. The corrugations were 75mm (2.95in) deep with a wavelength of 434mm (17.1in). The bend radius between the inclined fold and the longitudinal fold was 27mm (1.1in) and the corrugation angle was 36.9°. The web-to-flange fillet welds were 5mm (0.20in) in size. The stress range in the bottom flange varied from 64.7MPa (9.4ksi) to 131MPa (18.9ksi). The stress range was calculated at the top of the bottom flange using simple beam theory. Ibrahim (2001) reported that all six test specimens failed by fatigue cracking in the bottom flange within the constant moment region. Fatigue cracks initiated at the web-to-flange fillet weld toe along an inclined fold, and then propagated in the flange. The point of crack initiation generally occurred at the end of the inclined fold at the beginning of the bend region. In one case, the crack initiated at the weld toe in the middle of the inclined fold. This departure from typical behavior was attributed to a welding stop-start at the point of crack initiation. Multiple cracks were not reported.

To conclude this summary of previous research, the experimental results presented thus far are collectively plotted in Figure 3 with the mean S-N curves of the AASHTO LRFD fatigue categories. The figure suggests that the fatigue strength of corrugated web girders lies between the mean for Category B and the mean for Category C. The variability in

test results is attributed to various factors including variation in corrugated web geometry, specimen scale, actual stress conditions, fillet weld toe geometry, and so on.

Table 1. AASHTO fatigue categories.

Category	Constant A (MPa^3)	$log\ A$ (lower bound)	S	$log\ A$ (mean)	CAFL (MPa)
A	8.2×10^{12}	12.9138	0.221	13.3470	165
B	3.93×10^{12}	12.5944	0.147	12.8825	110
B′	2.00×10^{12}	12.3010	0.147[1]	12.5892	82.7
C	1.44×10^{12}	12.1584	0.063	12.2818	69
C′	1.44×10^{12}	12.1584	0.063[2]	12.2818	82.7
D	7.21×10^{11}	11.8579	0.108	12.0696	48.3
E	3.61×10^{11}	11.5575	0.101	11.7555	31
E′	1.28×10^{11}	11.1072	--	--	17.9

[1]Not provided in the original work by Keating and Fisher (1986); S assumed equal to that of Category B
[2]Not provided in the original work by Keating and Fisher (1986); S assumed equal to that of Category C

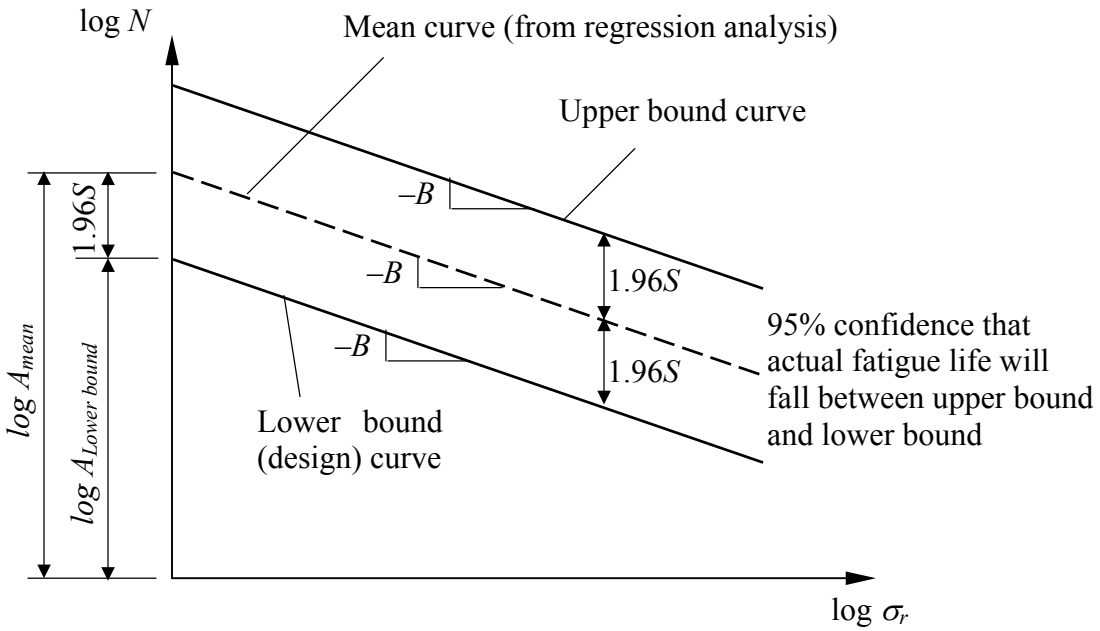

Figure 1. Relationship between mean, lower, and upper bound S-N curves.

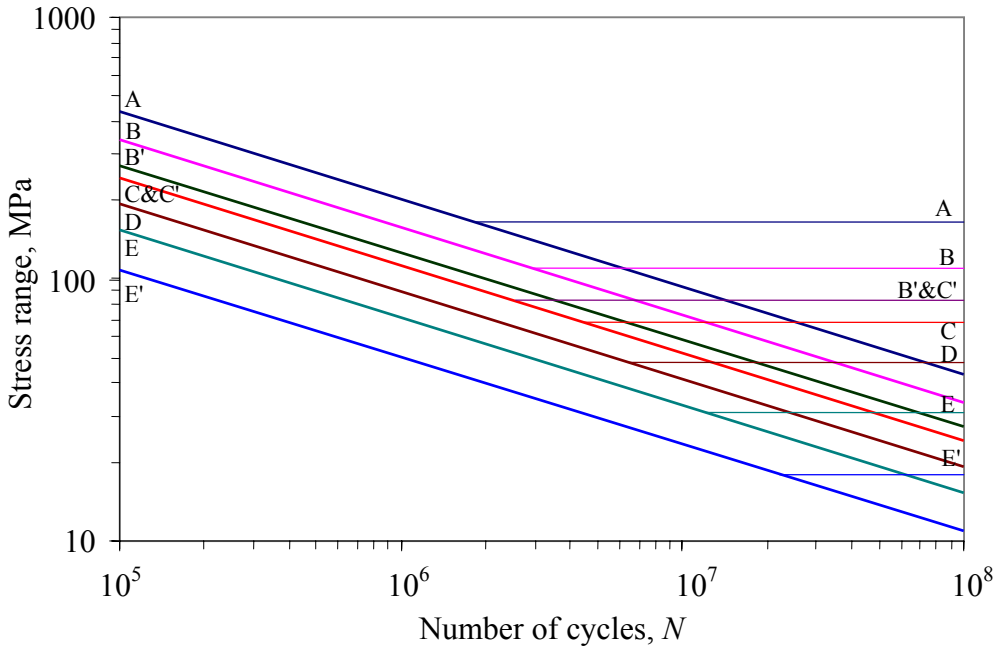

Figure 2. Design S-N curves for AASHTO LRFD fatigue categories.

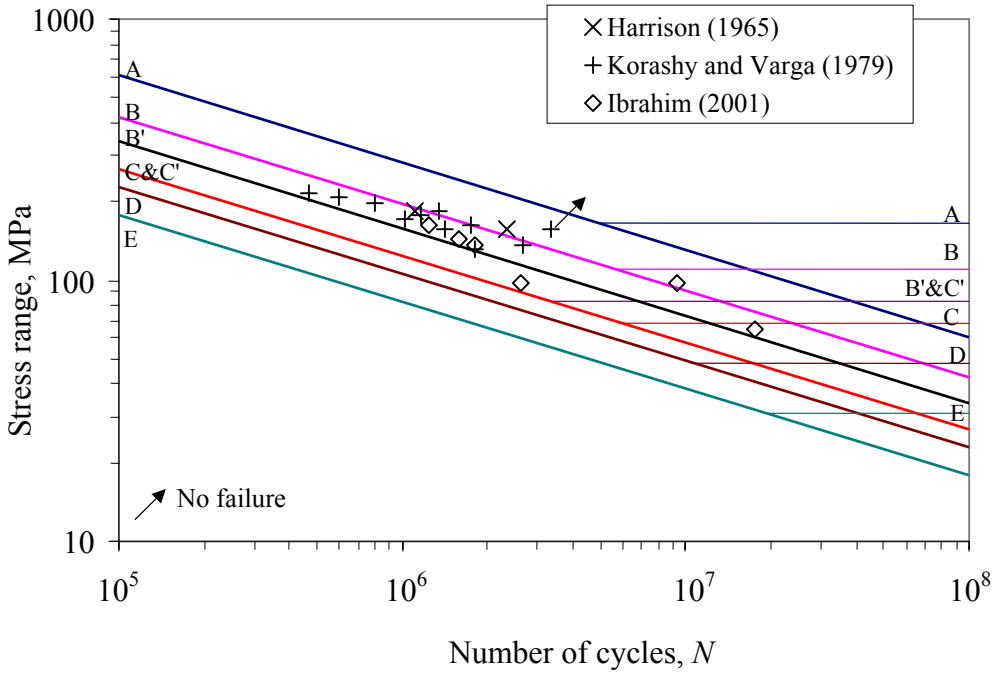

Figure 3. Mean S-N curves for AASHTO LRFD fatigue categories with test data from previous research.

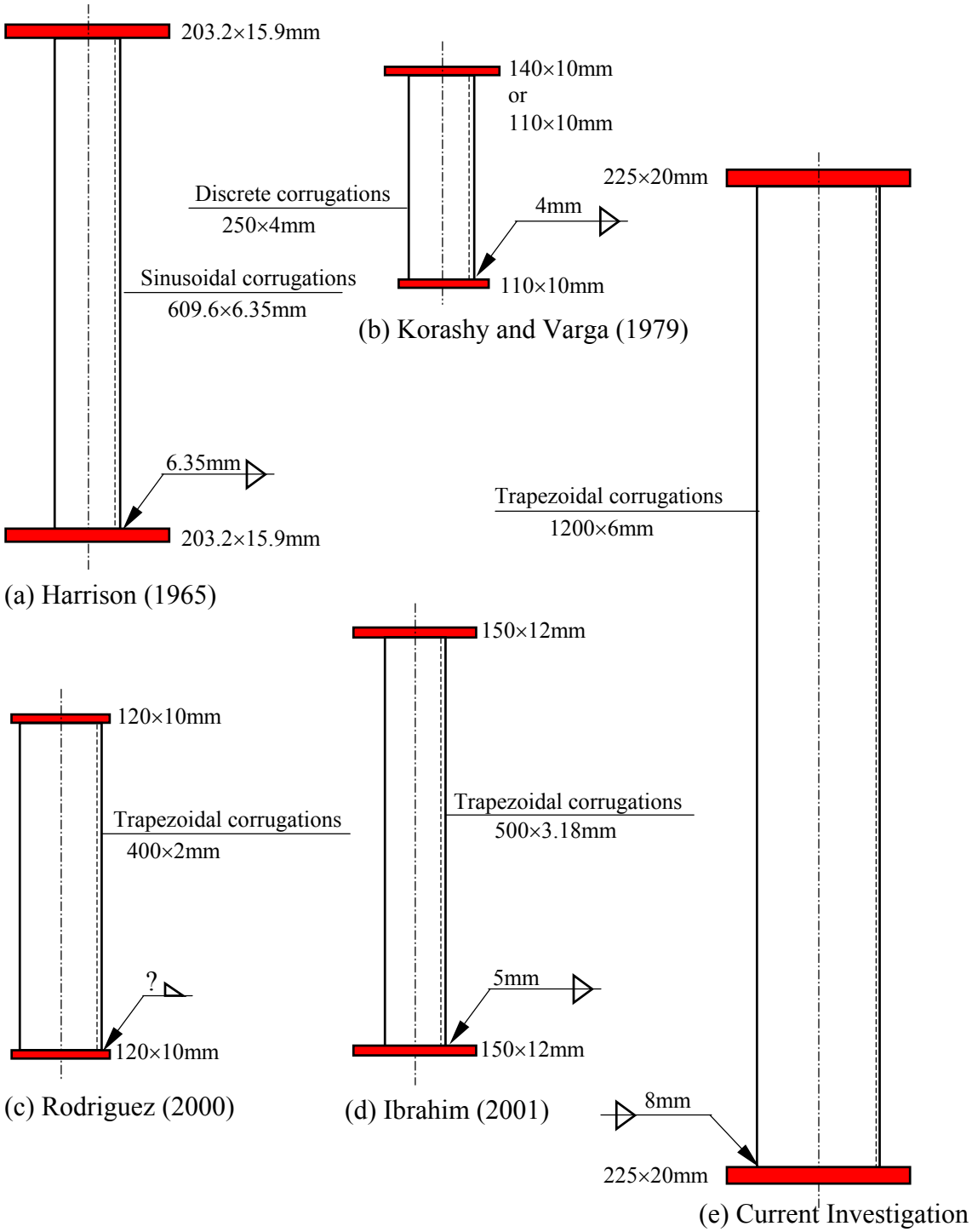

Figure 4. Corrugated web girder cross sections used in previous and the current experimental investigations (drawn to same scale).

3. Fatigue Strength Tests

3.1. Test Specimens

Previous experimental research used test specimens that were generally small in scale, and not necessarily representative of corrugated web girders for bridges. It is well established that small-scale specimens will generally result in a higher fatigue life than large-scale specimens (Fisher *et al.* 1970, Fisher *et al.* 1974, Keating and Fisher 1986). Keating and Fisher (1986) indicate that this trend can be attributed, in part, to reduced residual stress fields in small-scale specimens. Other factors include the size and frequency of weld-related defects, and the level of stress concentration.

Therefore, large-scale fatigue test specimens, representative of bridge girders, were used for the present study. The size of these fatigue test girder specimens was maximized under the constraints of budget and laboratory capabilities. Figure 5 shows the nominal geometry of the fatigue test girders. The fatigue test girders (denoted by G1A to G6A) were 7.4m (24.3ft) in length with an effective span of 7m (23.0ft) that consisted of seven corrugation wavelengths, each 1m (3.3ft) long. The web was 1.2m (3.9ft) deep and 6 mm (1/4in) thick. Both top and bottom flanges were 225mm (8.9in) wide and 20mm (13/16in) thick. A pair of 20mm (13/16in) thick stiffeners was provided at the reaction and load points to minimize local effects due to concentrated loads. The girders were designed for loading in four-point bending, with two loads and two reaction points, to produce a constant moment region between the load points, as shown in Figure 6.

Figure 4 compares the cross sections of fatigue test specimens tested by previous researchers with the cross section of the fatigue test girders used in the current investigation. The specimens tested by Harrison (1965), Korashy and Varga (1979), Rodriguez (2000), and Ibrahim (2001) are substantially smaller in size. In particular, for the previous specimens, the web thickness varied from 2mm (0.08in) to 6.4mm (1/4in), the web depth varied from 250mm (9.89in) to 610mm (24.0in), the flange thickness varied from 10mm (0.39in) to 15.9mm (0.63in), the flange width varied from 110mm (4.3in) to 203mm (8.0in), and the maximum reported web-to-flange fillet weld size was 6.35mm (0.25in).

Eight fatigue test specimens were fabricated. Six girders (denoted by G1A to G6A) were welded using semiautomatic GMAW, and two girders (denoted by G1B and G4B) were later re-fabricated from Girders G1A and G4A, and were re-welded using robotic GMAW. GMAW was used because of its potential for use in automated welding. The main purpose of testing robotically welded girders was to evaluate the effect of welding process on the fatigue resistance.

A full-scale corrugated web was used in the test specimens. The corrugated web profile (geometry) of the test specimens is shown in Figure 7. This web corrugation geometry was developed based on static shear strength considerations as discussed by Sause *et al*. (2003). Two features of this geometry, however, were selected with the fatigue performance in mind, namely, the corrugation angle, α, and the bend radius, r.

Previous research suggests that the fatigue life increases as α decreases. However, to meet the shear strength requirements, a minimum value of α is required. Lindner and Huang (1995) suggest that α should not be less than 30° for the corrugation folds to provide adequate support for one another along the fold lines to mobilize the full shear capacity. The trapezoidal web geometry of the test specimens has a corrugation angle, α, of 36.9°, which is slightly larger than 30°.

The second important feature of the trapezoidal web geometry is the use of a bend radius, r, of 120mm (4.7in), which gives an r/t_w ratio of 20. This large bend radius has two main effects: (1) maintaining good fracture toughness characteristics in the bend region of the web, and (2) enhancing the fatigue life. Good fracture toughness in the bend region is maintained by reducing the plastic deformations in the web arising from the web forming process. It can be shown that the maximum plastic strain of the web in the bend region of the test specimens is 2.5% (Abbas 2003). It is believed, based on the work of Kaufmann *et al.* (2001), that this level of plastic strain produces only a small reduction in the fracture toughness in the bend region. Another favorable effect of using a large bend radius is reducing the stress concentrations at the web-to-flange fillet weld toe in the bend region under fatigue loading. If a small bend radius is used, the sudden change in geometry will result in high stress concentrations at the web-to-flange weld toe in the bend region. This result was shown by Ibrahim (2001), who reported fatigue cracks initiating from the weld toe in the bend region when the bend radius ratio, r/t_w, was 8.5.

A web-to-flange weld size of 8mm (5/16in) was used even though a weld size of 6mm (1/4in) would have been sufficient to satisfy strength requirements. A larger weld size leads to larger internal weld defects, increased residual stresses, and larger stress concentration factors at the weld toe, all of which can lead to a reduced fatigue life (Fisher *et al.* 1970 and Fisher *et al.* 1974). The minimum fillet weld size allowed by the AASHTO LRFD specifications is 6mm (1/4in). A weld size of 8mm (5/16in) is the maximum size that the fabricator could provide in a single pass. The fillet weld was undermatched with a yield strength of 345MPa (50ksi).

The fabricator of the fatigue test girders was instructed to avoid welding stop-starts within the web bend region (Sause 2003). Defects associated with welding stop-starts are usually detrimental and should be avoided, especially in the bend region. Most of the welding stop-starts were located on the longitudinal fold and occasionally on the inclined fold.

Girders G1B and G4B were re-fabricated from Girders G1A and G4A. After the fatigue tests of Girders G1A and G4A were completed, the damaged bottom (tension) flange was removed using plasma cutting. The cut was made in the longitudinal direction in the web approximately 50mm (2in) above the upperside of the bottom flange. Manual grinding was subsequently used to treat the cut edge. After this process was completed a new bottom flange, also made of ASTM A709 HPS-485W (HPS-70W) steel (ASTM 2001) and with approximately the same dimensions, was robotically welded to the web. A photograph of the robotic welding is shown in Figure 8.

Robotic welding is considered to be ideal for fabricating corrugated web I-girders for bridges. Advantages include: (1) an automated and programmable process, (2) automated tracking of the web geometry, (3) excellent control of weld parameters, (4) weld uniformity, and (5) an enhanced weld toe geometry. An example of the quality of robotic fillet welds is shown in Figure 9. The superiority of robotic welds over semiautomatic welds was apparent by visual examination, especially regarding the weld toe geometry.

In designing the fatigue test girders several constraints were considered. The available budget, the total number of test specimens, and the testing equipment were predetermined in the project planning stages. The size of the test girder flanges was based on the capacity of the loading equipment and the required stress ranges. The resulting flanges were especially susceptible to flange transverse bending due to shear as well as secondary effects such as flange distortion and non-uniform web contribution to flexure. All of these effects are described in detail by Abbas (2003). These effects resulted in significant differences between the nominal stresses (based on conventional beam theory from overall bending) and the actual stresses. The effect of flange transverse bending due to shear was particularly pronounced in the shear span outside of the constant moment test region (Figure 6) and a special weld treatment (described below) was used in this region. Even within the constant moment region, between the two load points, where the overall shear is zero, the stresses in the flange varied as described by Abbas (2003). In future fatigue tests, larger flanges, which will reduce the differences between the nominal and bending stresses and the actual stresses, are suggested. However, fatigue tests of specimens with larger flanges will require more sophisticated testing equipment, longer testing time, and significantly increased testing cost.

Abbas (2003) shows that the flange stresses at some locations within the shear region of the fatigue test specimens were substantially higher than the stresses within the constant moment region due to flange transverse bending. Using the analytical methods developed by Abbas (2003), the locations where the flange stresses are high were identified (Figure 10) and treated using ultrasonic impact treatment (UIT). UIT is a fatigue strength enhancement technique, conceptually similar to air hammer peening, that was developed by Statnikov (1997) and studied at Lehigh University (Takamori and Fisher 2000). The UIT equipment consists of a handheld tool and an ultrasonic generator. The details of the equipment are proprietary. The weld improvement is achieved by the introduction of beneficial residual compressive stresses, and the reduction in geometric stress concentrations at the weld toe. UIT was applied to the weld toe on the bottom flange at the locations shown in Figure 10 for each test specimen. UIT successfully prevented fatigue cracks in the treated locations during the fatigue tests.

Bearing stiffeners of the fatigue test girders were located at the center of the inclined folds (Figure 5) based on a recommendation by Elgaaly *et al.* (2000) and Rodriguez (2000). Partial depth stiffeners at the loading points were included for testing purposes. A bridge girder with corrugated webs requires bearing stiffeners only at the reaction points. No other stiffeners are needed, however cross frame connection plates are needed.

3.2. Test Setup, Instrumentation and Procedure

The fatigue test girders were tested in the dynamic test bed of Fritz Engineering Lab at Lehigh University. The main characteristics of the test setup are shown in the photograph of Figure 11. The specimens were mounted on two stiffened steel pedestals as shown. The bearings allowed for the free extension of the bottom flange at one end, thus simulating the intended simply supported boundary conditions.

The load jacks were driven by oil-pumping pulsators that were coupled to ensure synchronization. The operating capacity for each jack was 489kN (110kips). Two braced steel frames provided the required support for the jacks. Additionally, the load points were braced in the transverse direction. The girders were tested in 4-point bending (Figure 6), thus producing a region of constant moment and zero shear between the two load points, which were 3m (9.8ft.) apart and were symmetrically positioned about midspan. The loads were applied at a speed of 261cycles/min (4.35Hz). Two load cells, one at each jack location, measured the applied loads.

The test matrix is given in Table 2 in the order in which the girders were tested. The main variables of the test matrix are the stress range and the welding procedure. The nominal stress range varied from 103MPa (15.0ksi) to 138MPa (20.0ksi). Tests of identical girders at the same stress range were intended to provide repeatable results. The nominal stress was defined as the longitudinal stress on the top surface of the tension flange calculated according to simple beam theory using overall bending moment only. The measured cross-sectional dimensions were utilized in calculating the nominal stress, and the web contribution to flexure was neglected for reasons discussed in Sause *et al*. (2003).

The magnitude of applied loads was determined from the predefined nominal stresses. The minimum load per jack was 44.5kN (10.kips), which corresponds to a minimum nominal stress of approximately 15MPa (2.2 ksi). The maximum load per jack was selected to provide a maximum stress needed to reach the predefined nominal stress range. This arrangement gave a stress ratio, R, that varied between 0.10 and 0.13, as shown in Table 2.

Strain gages were placed near locations where fatigue cracks were likely to occur. Two schemes were used as shown in Figure 12. The first scheme (Figure 12a) was used for Girder G2A, which was the first girder tested. In this scheme, strain gages were provided near the bend region in anticipation of fatigue cracks near this location. Test results later showed that the majority of fatigue cracks initiated along the inclined fold. The second scheme, shown in Figure 12b, was used for Girders G1A and G3A to G6A. In this scheme, pairs of gages were placed at the transverse section at the middle of the inclined fold, 51mm (2in) from the centerline as shown. The gages were placed on longitudinal axes passing through the nominal ends of the flat portion of the inclined folds. The two gages at the same transverse section were used to estimate the stress variation across the width of the flanges as shown in Figure 13.

The strain gage plan for Girder G2A is shown in Figure 14. All strain gages were located on the flanges and were oriented in the longitudinal direction as shown. Seven sections along the span (four within the shear regions and three within the constant moment region) were instrumented with gages that were, whenever possible, provided in pairs to enable the middle surface strains to be estimated. The strains were used to study flange transverse bending and plate bending behavior.

The remaining strain gages were provided near the corrugation corners and on the top of the bottom flange in accordance with the scheme shown in Figure 12a. Note that all strain gages were either placed along the flange centerline or adjacent to the flange edge at a distance of approximately 13mm (0.5in) from the edge. The strain gage plan for Girder G1A and Girders G3A to G6A is given in Figure 15. As shown, strain rosettes were used at selected locations to verify the 2-D state of stress. Except at midspan, the strain gages were located only on the top of the bottom flange.

Prior to the beginning of each test, several static cycles were conducted to verify the functionality of the instrumentation. For the static tests, the girders were loaded up to a load level of 489kN (110.kips) per jack. The tests were run continuously when possible. The girders were inspected periodically for cracks by naked eye, using magnifying glasses, and by liquid penetrant techniques. The frequency of inspection varied from once every 12 hours, at times when cracks were not expected, to continuous inspection at times when multiple cracks were initiating and girders were approaching their fatigue life. The tests were terminated after the fatigue crack had reached the flange edge.

Table 2. Test matrix.

Girder	Nominal Stress Range[1] (MPa)	Stress ratio, R $= P_{min}/P_{max}$ or $= \sigma_{min}/\sigma_{max}$
G2A	138	0.10
G1A	138	0.10
G4A	138	0.10
G5A	103	0.13
G6A	103	0.13
G3A	103	0.13
G4B	138	0.10
G1B	110	0.12

[1] At the top surface of the tension flange in the longitudinal direction based on simple beam theory

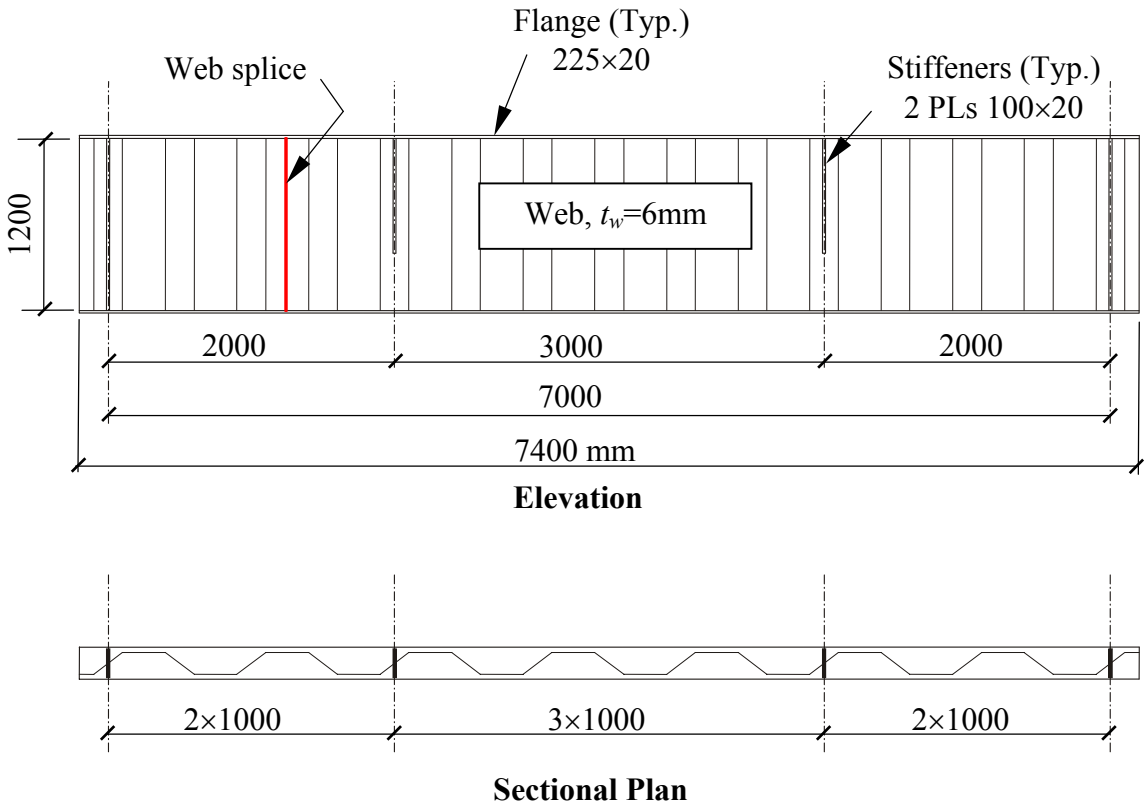

Figure 5. Fatigue test specimens (Girders G1A to G6A).

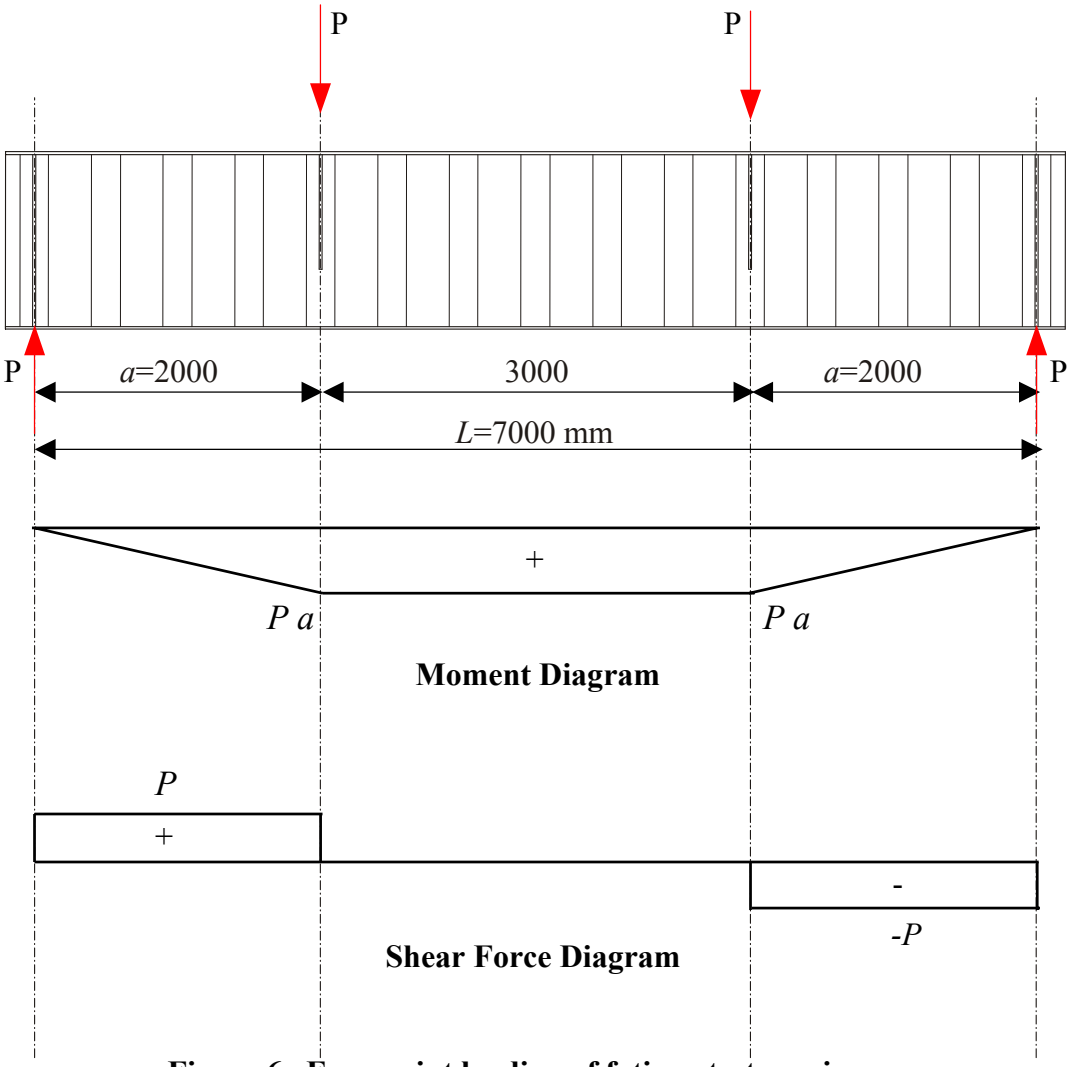

Figure 6. Four point loading of fatigue test specimens.

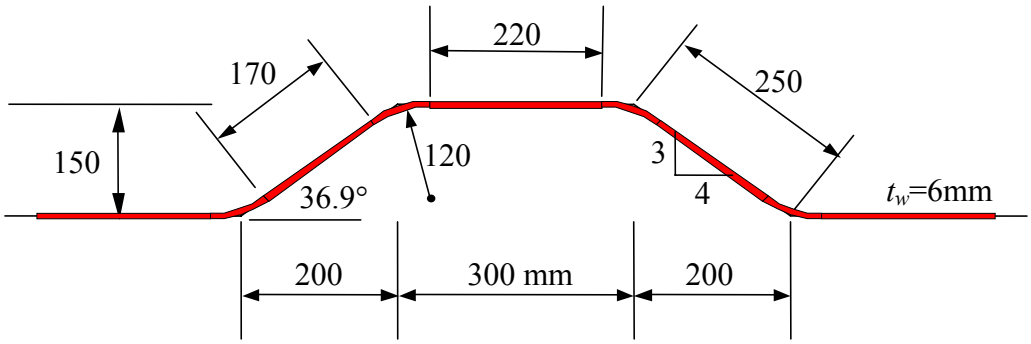

Note: dimensions are measured to middle surface of web plate

Figure 7. Corrugated web geometry of test specimens.

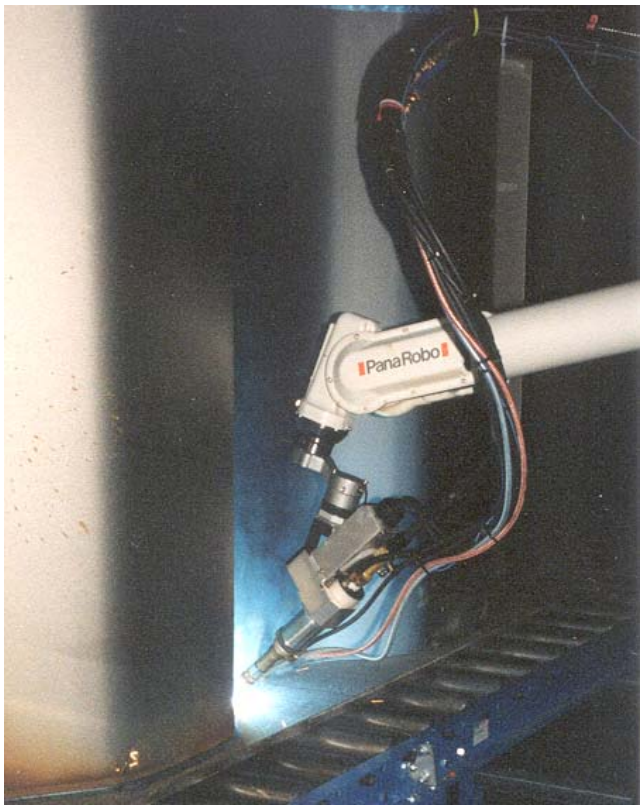

Figure 8. Robotic welding.

Figure 9. Robotically made fillet weld.

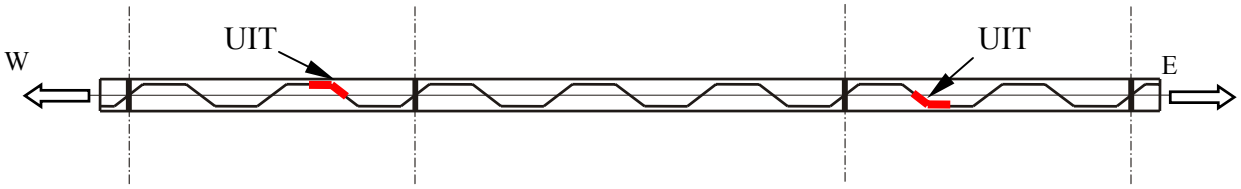

Figure 10. Locations of UIT of web-to-bottom-flange fillet weld.

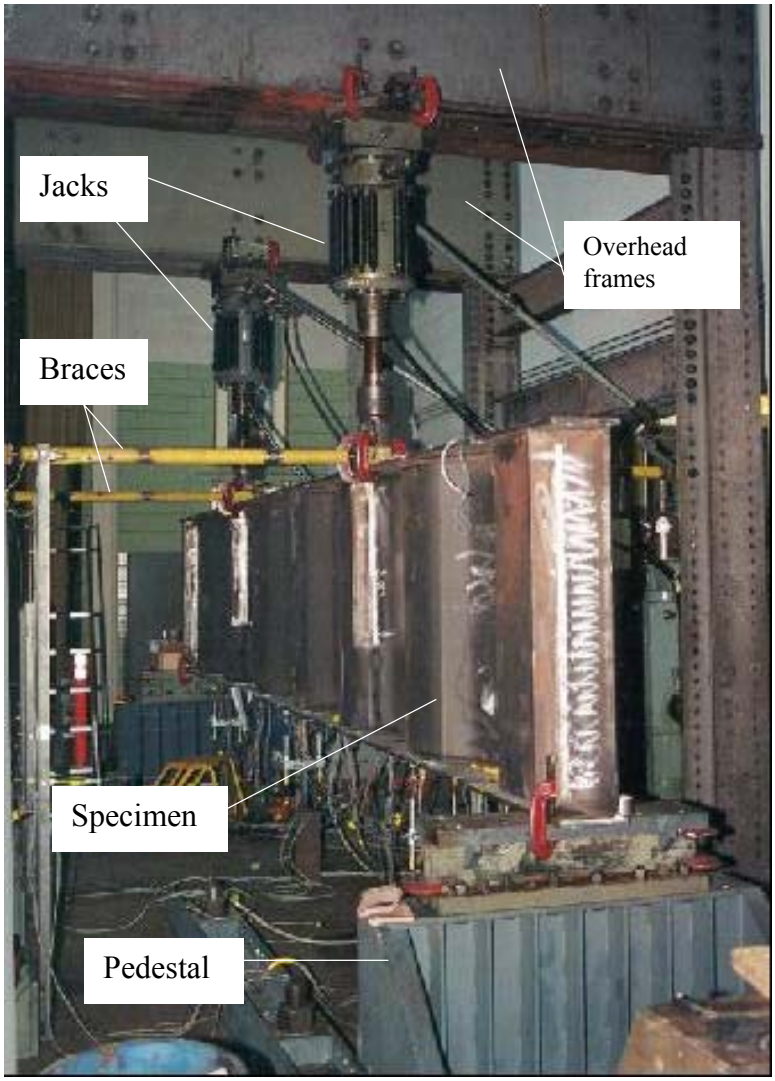

Figure 11. Fatigue test setup.

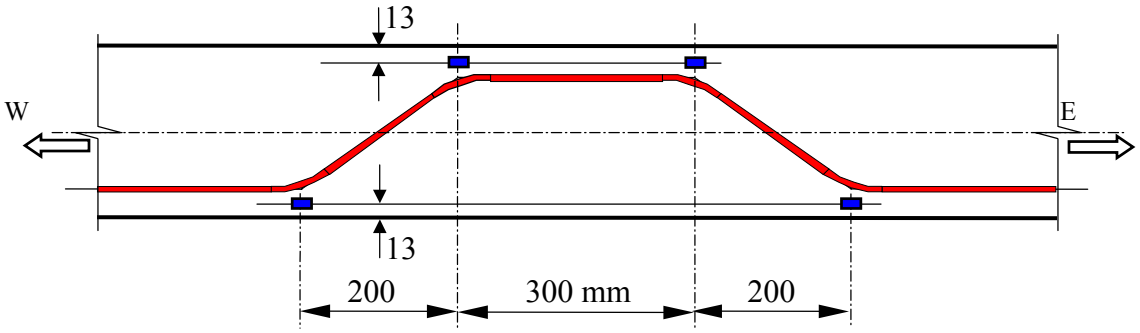

(a) Girder G2A

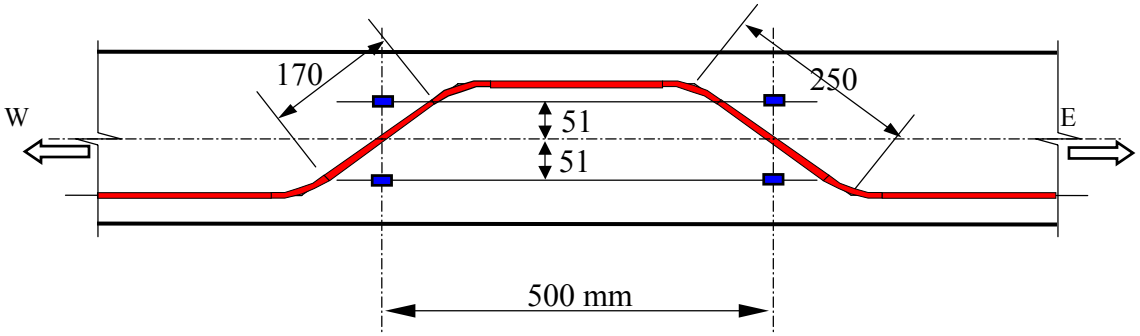

(b) Girders G1A and G3A to G6A

Strain gage (bonded on the top surface of the bottom flange)

Figure 12. Typical strain gage locations for fatigue tests.

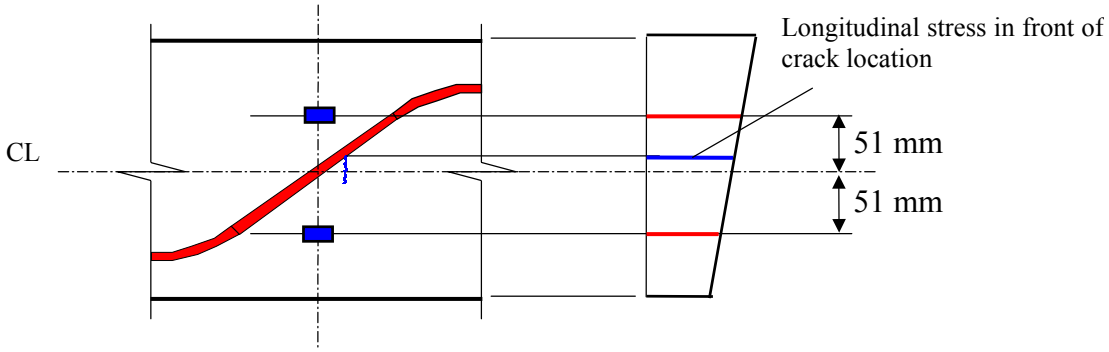

Figure 13. Longitudinal stress distribution across flange width.

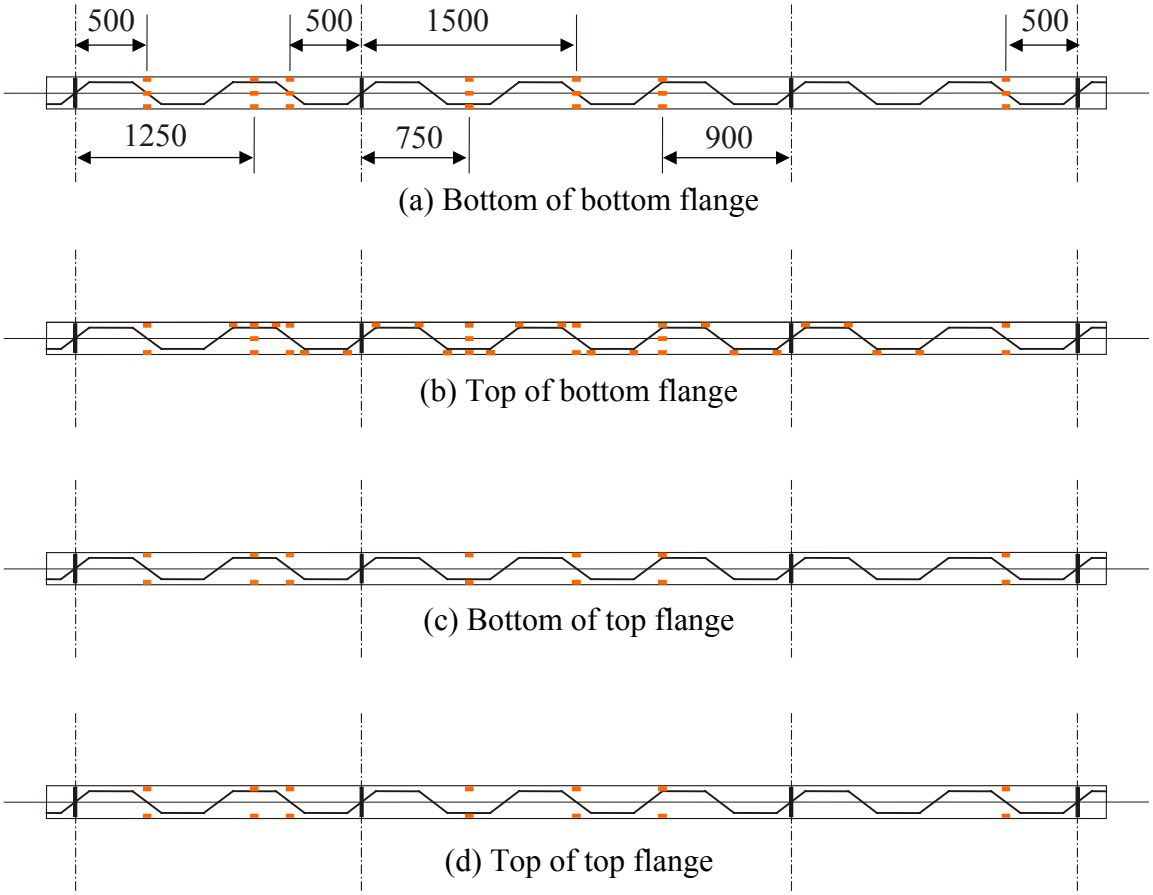

Notes
All dimensions are in mm
Strain gages near flange edges are 13mm from the edge

Legend
- Longitudinal strain gage

Figure 14. Strain gage plan for Girder G2A.

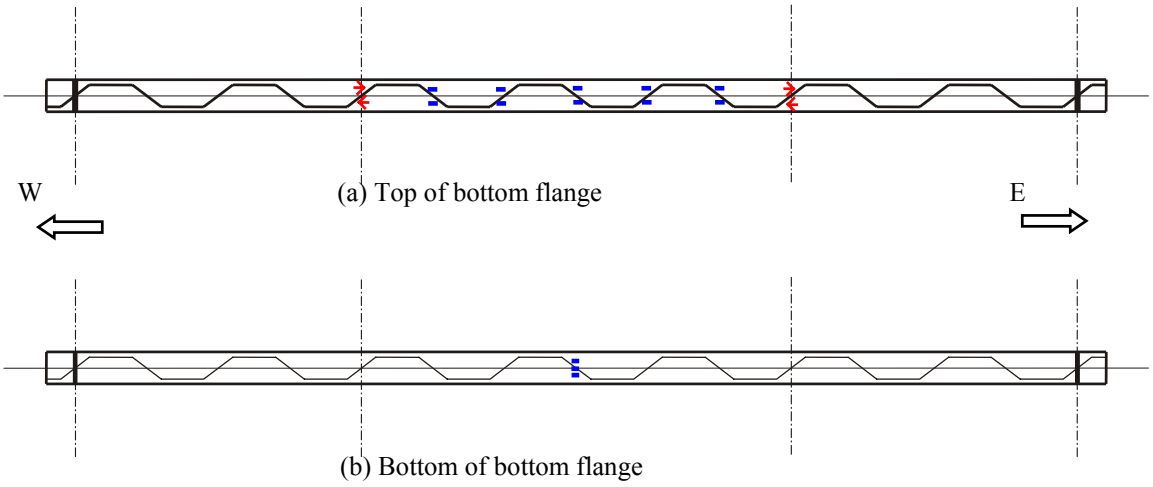

Notes
Off-center strain gages are 51 mm from flange centerline
See Figure 12(b) for detailed strain gage locations

Legend
- Three-element strain rosette
- Uniaxial strain gage

Figure 15. Strain gage plan for Girders G1A and Girders G3A to G6A.

4. Fatigue Strength Test Results

4.1. Load and Strain Measurements

The loading and strain gage data were acquired twice a day when the specimen was continuously running (*i.e.,* once every 12 hours or approximately every 188,000 cycles). The measured load range was used to verify compliance with the target load range. The load range was used to control the tests. The measured strain ranges were subsequently transformed into stress ranges. For uniaxial strain gages, the stresses were obtained from the measured strains using:

$$\sigma = E\varepsilon \tag{3}$$

where, E is Young's modulus of elasticity. A value of E equal to 202,500MPa (29,400ksi) was used. For strain gage rosettes, it was possible to determine the 2-D state of stress as follows. First, the strains, ε_z, ε_x, and γ_{zx} were determined from rosette strains using a 2-D strain transformation. Then, assuming plane stress conditions, the stresses σ_z, σ_x, and τ_{zx} were calculated from the generalized Hooke's law, as follows:

$$\begin{aligned} \sigma_z &= \frac{E}{1-\upsilon^2}\left[\varepsilon_z + \upsilon\varepsilon_x\right] \\ \sigma_x &= \frac{E}{1-\upsilon^2}\left[\varepsilon_x + \upsilon\varepsilon_z\right] \\ \tau_{zx} &= G\gamma_{zx} \end{aligned} \tag{4}$$

where, υ is Poison's ratio, which was taken as 0.3, and G is the shear modulus of elasticity which is given by:

$$G = \frac{E}{2(1+\upsilon)} \tag{5}$$

The measurements showed that the longitudinal stresses on the top surface of the bottom flange were generally larger than the nominal stresses. This behavior is a result of flange plate distortion as described by Abbas (2003). The strain gage measurements also showed that the state of stress in the flanges was not purely uniaxial. The angle of the major principal stress varied between 2° and 11° from the longitudinal direction. Nevertheless, it was found that the difference between the longitudinal stress and the principal stress was very small, and, for practical purposes, Equation 3 can be used to calculate the longitudinal flange stresses from the longitudinal strains.

4.2. Test Observations

Girders G2A, G1A, and G4A were tested, in that order, at a nominal stress range of 138MPa (20.0ksi). A summary of the results is given in Table 3. All girders from this group of fatigue specimens failed due to a fatigue crack that propagated from the intersection of the web-to-flange fillet weld with the bottom (tension) flange within the constant moment test region. The number of cycles to failure, *N*, varied from 1,303,500 cycles for Girder G4A to 1,448,000 cycles for Girder G1A with an average fatigue life of 1,389,900 cycles. The scatter in the test data at this stress range (138MPa (20.0ksi)) is rather small.

The fatigue cracks in Girders G2A, G1A, and G4A were generally detected after approximately 1 million cycles. Using liquid penetrant techniques, it was possible to observe cracks as small as 1mm (0.04in) to 2mm (0.08in) in size. These cracks originated at the intersection of the web-to-flange fillet weld with the bottom flange. Many cracks were observed along the inclined web folds and parts of the bend region adjacent to the inclined folds. For this group of test specimens, nearly simultaneous initiation of multiple cracks on several different inclined folds was observed. Fatigue cracks were not detected along the longitudinal folds. Figure 16 shows the typical multiple crack pattern along the inclined fold. The figure shows that the point of fatigue crack initiation was usually associated with a non-uniform weld toe geometry introduced by the semiautomatic GMAW process. The semiautomatic GMAW process uses manual manipulation of a welding gun with an automatically fed electrode, and results in an undulating weld geometry. These undulations are referred to as weld ripples.

The fatigue cracks propagated in the flange at an angle that was approximately 10° from perpendicular to the longitudinal axis. This observed angle is consistent with the principal stress angle, determined from the strain gage rosettes. The observed crack growth rate varied from one crack to another. Some cracks appeared to be shielded by nearby cracks, thus causing them to propagate at a slower rate. Other cracks seemed to grow unimpeded. Eventually one crack became the main crack, propagated through the flange thickness and then to the flange tip causing the tests to be terminated. Photographs of the main fatigue cracks of Girders G2A, G1A and G4A, are shown in Figures 17, 18, and 19, respectively. Although multiple cracks were observed at locations along the inclined folds, the main cracks seemed to occur near the end of the inclined fold (*i.e.,* near the bend region).

A careful posttest survey of fatigue cracks was conducted and the results are given in Table 4. To facilitate discussion of the cracks, the longitudinal web folds are numbered 1 through 14 as shown in Figure 20. The inclined web folds are identified using the adjacent longitudinal folds. For example, Fold 1-2 means the inclined fold between longitudinal Fold 1 and longitudinal Fold 2. Table 4 shows that fatigue cracks were observed in the bottom flange along nearly every inclined fold within the constant moment test region on the north and the south side alike. The number of observed cracks varied from 41 cracks for Girder G2A to 54 cracks for Girder G4A. The abundance of

cracks is a strong indication that the girders attained their fatigue strength and reduces concerns about stress variability within the test region.

Girders G5A, G6A, and G3A were tested, in that order, at a nominal stress range of 103MPa (15.0ksi). A summary of the results is given in Table 3. For this group of test specimens, nearly simultaneous initiation of multiple cracks on several different folds did not typically occur. Therefore, certain cracks, that occurred under conditions that were different than typical conditions in the specimen, were repaired as follows.

Girder G5A developed two closely spaced fatigue cracks in the bottom flange at the weld toe on the north side of Fold 9-10 after approximately 1,992,200 cycles. Both cracks were approximately 6.4mm (0.25in) in length. The stress conditions near these cracks were calculated from strain measurements in the flange near Fold 9-10, and it was found that the longitudinal stress range in front of the crack location was approximately 120.MPa (17.4ksi). This stress range was 16% greater than the nominal stress range for Girder G5A, and was also substantially higher than the stress ranges determined from strain gages at other locations within the constant moment test region on the bottom flange. It is worth noting that the web was visibly misaligned in the region of Fold 9-10. Consequently the cracks on the north side of Fold 9-10 were repaired.

Initially, the repair used plates clamped to the bottom flange to reduce the stresses by reinforcing the area near the cracks. Unfortunately, the stress states in neighboring folds were also disrupted and the method of repair by clamping was discarded. Instead, the cracks were repaired by grinding to eliminate the crack tip, followed by air hammer peening to introduce beneficial compressive residual stresses. The grinding and peening repair method worked well and the test was consequently resumed. Girder G5A survived 7,316,500 cycles without failure before the test was discontinued. Posttest inspection did not reveal any additional cracks in the bottom flange.

Girder G6A developed a small fatigue crack in the bottom flange at the weld toe on the north side of Fold 6-7 after 1,895,100 cycles. Visual inspection showed that the crack initiated from what appeared to be a weld stop-start location. The longitudinal stress range in the flange in front of the crack location was determined to be 109MPa (15.9ksi), only slightly higher than the nominal stress range. The test was resumed and five more cracks were detected in the flange along three different inclined folds. All six fatigue cracks occurred on the north side of the web as discussed below. The presence of several cracks suggested that this particular girder had reached its fatigue strength. The cracks were not repaired and the test was resumed until failure occurred at 2,563,400 cycles. The crack that caused failure propagated from a weld stop-start location in the web bend region. Figure 21 shows a photograph of the main fatigue crack of Girder G6A.

It is important to note that the web-to-flange fillet weld quality was inconsistent for Girder G6A. The fabricator confirmed that two different certified welders worked on Girder G6A. Figure 22 shows close-up photographs of the fillet welds on different sides of Fold 8-9. The fillet weld quality is substantially better on the south side (Figure 22b) than on the north side (Figure 22a), where the weld geometry is clearly less uniform.

These results show that the weld geometry produced by semiautomatic GMAW may have a significant impact on the fatigue strength. If the weld quality on the north side of Girder G6A had been as good as on the south side, then it is expected that Girder G6A would have attained a longer, and perhaps infinite, fatigue life.

The observed results for Girder G3A are similar to those of G5A. An approximately 2mm (0.08in) long fatigue crack was detected in the flange at the weld toe along Fold 8-9 after 1,992,200 cycles. The crack was allowed to grow until it became 12.7mm (0.5in) long at 3,436,100 cycles, after which it was repaired by grinding and peening. The test was subsequently resumed and Girder G3A survived 7,645,100 cycles without failure before the test was discontinued. Posttest inspection did not reveal any additional cracks in the bottom flange.

Girder G4B was tested at a nominal stress range of 138MPa (20.0ksi) to evaluate the effect of robotic welding on the fatigue performance. Girder G4B survived 1,980,000 cycles before it failed from fatigue cracking of the bottom flange as shown in Figure 23. As shown in the figure, several fatigue cracks in the flange coalesced just prior to failure. The fatigue cracks initiated from the fillet weld toe along the inclined fold. The use of a robotic GMAW process resulted in an increase of approximately 42% in fatigue life compared to girders welded using semiautomatic GMAW. It is believed that increased uniformity in the weld toe geometry of the robotically-made welds is responsible for the observed longer fatigue life.

Girder G1B was tested at a nominal stress range of 110.MPa (16.0ksi). This girder was tested at a slightly higher stress range than Girders G5A, G6A, and G3A to determine if Category B of the AASHTO LRFD specifications, with a CAFL of 110.MPa (16.0ksi), could be attained. Multiple cracks were found at 2,800,000 cycles along Fold 7-8 where the stress range was approximately 125MPa (18.2ksi), 14% greater than the nominal stress range of 110.MPa (16.0ksi). These cracks were repaired by grinding and peening, and the test was resumed. Girder G1B failed finally after 3,500,000 cycles from a weld stop-start at the middle of a longitudinal web fold. A photograph of the failure is shown in Figure 24.

4.3. Fracture Surfaces

The fatigue cracks observed during and after the tests appeared to have initiated from the fillet weld toe. This observation was verified by examining the fracture surface of the main cracks to ensure that weld internal defects were not responsible for crack initiation. Examination of the fracture surfaces showed the influence of the weld toe geometry on the fatigue crack propagation. Only the girders welded using semiautomatic GMAW were studied. As mentioned earlier, the GMAW process uses manual manipulation of a welding gun with an automatically fed electrode, and results in undulations in the weld geometry referred to as fillet weld ripples.

The fracture surface examination suggested three main stages of crack life: (1) crack initiation at the weld toe, (2) crack propagation into the flange along the weld toe, and (3) crack propagation into the flange away from the weld toe. The three stages are schematically represented in Figure 25.

As seen in the figure, fatigue crack initiation (stage 1) generally occurred at the toe of the web-to-flange fillet weld where the surfaces of two weld ripples intersect with the flange surface. The angle between the flange longitudinal axis and the tangent to the intersection of the weld surface with the flange surface at the weld toe, α_{int}, tends to be largest at this location. From measurements made on the fracture surface for Girders G2A and G4A, it was found that α_{int} at the crack initiation point was approximately 70° as shown in Figure 25. Previous fatigue studies suggest that the stress concentration at a fillet weld toe will be largest when the weld toe is perpendicular to the applied stress direction. It follows that fatigue crack initiation is likely to occur where the intersection of the weld surface with the flange surface is closest to perpendicular to the principal stress direction at the flange surface.

Stage 2 is characterized by crack propagation along the weld toe. The propagation along the weld toe was usually several millimeters in length (5mm (0.20in) for G2A and 7mm (0.28in) for G4A) as shown in Figure 25. The fatigue crack surface associated with stage 2 was non-uniform and it was not possible to determine from the fracture surface a clear pattern of fatigue crack propagation during stage 2. However, the short crack propagation length during stage 2 suggests that the extent of propagation through the flange thickness is small during this stage. In the final stage of propagation (stage 3), the fatigue crack turns into the flange and propagates perpendicular to the principal stress direction. From measurements made on the fracture surface for Girders G2A and G4A, it was found that α_{int} at the beginning of stage 3 was approximately 50° as shown in Figure 25.

The different stages of crack growth for the main crack of Girder G2A are illustrated in the close-up photograph of Figure 26. Examination of the fracture surface reveals the presence of a secondary crack, such as the one shown in Detail B of Figure 25. This secondary crack started at the weld toe at point '*b*' (Figure 25). At point '*c*', however, the secondary crack ceased to propagate, perhaps because it was shielded by the faster growing neighboring main crack. Eventually, the two cracks joined along the coalescence plane from point '*c*' to point '*d*' and propagated toward '*e*' as shown in Detail B of Figure 25. Thus, Figure 26 shows the fracture surface along '*abcde*' and not '*afde*' as shown in Detail B of Figure 25.

The fracture surface of the main crack of Girder G4A was similarly examined as shown in Figure 27. Crack propagation "beach" marks are readily visible on the fracture surface and are semi-elliptical in shape, suggesting that the crack propagation pattern can be idealized as shown in Figure 28. The ratio of the minor axis of the ellipse to the major axis of the ellipse was found to be rather constant and approximately equal to 0.75.

Inspection of several fracture surfaces from the test specimens using the naked eye, a magnifying glass, and a scanning electron microscope (SEM), indicated that none of the cracks originated at internal defects within the fillet welds. The evidence confirms that the cracks initiated at the fillet weld toe. The crack initiation and propagation patterns were influenced by the characteristics of the weld toe geometry. In particular, the influence of weld ripples on crack initiation (stage 1) and subsequent crack propagation (stage 2) was evident.

The crack initiation and propagation features described above are complex. Only stage 3 of crack propagation was idealized for analysis. However, stages 1 and 2 seem to depend on the weld toe geometry and the corrugation angle.

Table 3. Summary of test results.

Girder[1]	Nominal Stress Range[2] (MPa)	No. of Cycles to Failure, *N*	Crack Location
G2A	138	1,418,100	Flange from fillet weld toe along inclined fold
G1A	138	1,448,000	Flange from fillet weld toe along inclined fold
G4A	138	1,303,500	Flange from fillet weld toe along inclined fold
G5A	103	>7,316,500	No failure
G6A	103	2,563,400	Flange from fillet weld toe along inclined fold
G3A	103	>7,645,100	No failure
G4B	138	1,980,000	Flange from fillet weld toe along inclined fold
G1B	110	3,500,000	Flange from fillet weld at start-stop location along longitudinal fold

[1] 'A' and 'B' denote semiautomatic GMAW and robotic GMAW welding respectively
[2] At the top surface of the tension flange in the longitudinal direction based on simple beam theory

Table 4. Posttest survey of fatigue cracks in Girders G2A, G1A, G4A and G6A.

Inclined Fold	G2A		G1A		G4A		G6A	
	North	South	North	South	North	South	North	South
1-2	--	--	--	--	--	--	--	--
2-3	--	--	--	--	--	--	--	--
3-4	--	--	--	--	--	--	--	--
4-5	1	6	3	--	1	1	1	--
5-6	--	5	4	1	1	2	--	--
6-7	3	4	4	1	10	3	2	--
7-8	1	5	6	7	4	5	--	--
8-9	6	4	2	1	4	4	1	--
9-10	1	1	4	4	7	2	--	--
10-11	4	--	2	4	9	1	2	--
11-12	--	--	--	--	--	--	--	--
12-13	--	--	--	--	--	--	--	--
13-14	--	--	--	--	--	--	--	--
Total	16	25	25	18	36	18	6	--
	41		43		54		6	

(a) Girder G2A

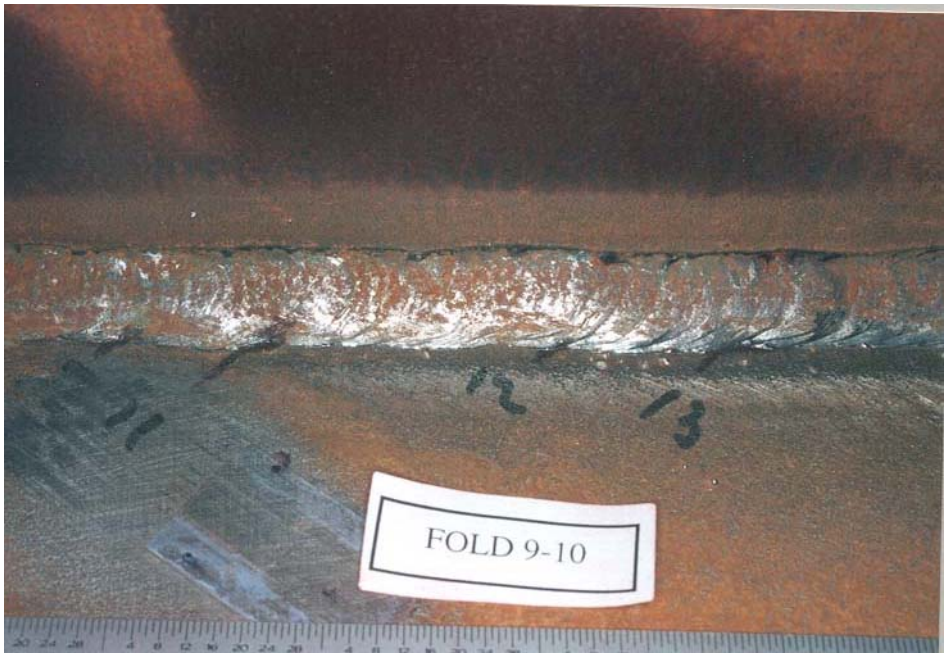

(b) Girder G1A

Figure 16. Examples of multiple fatigue cracks at fillet weld toe.

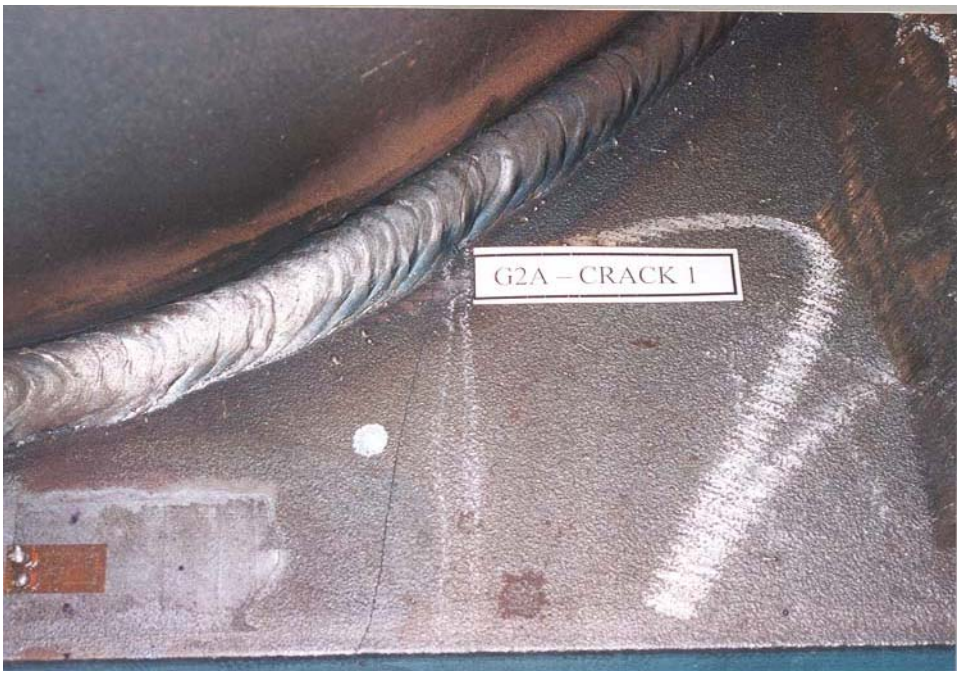

Figure 17. Main fatigue crack of Girder G2A.

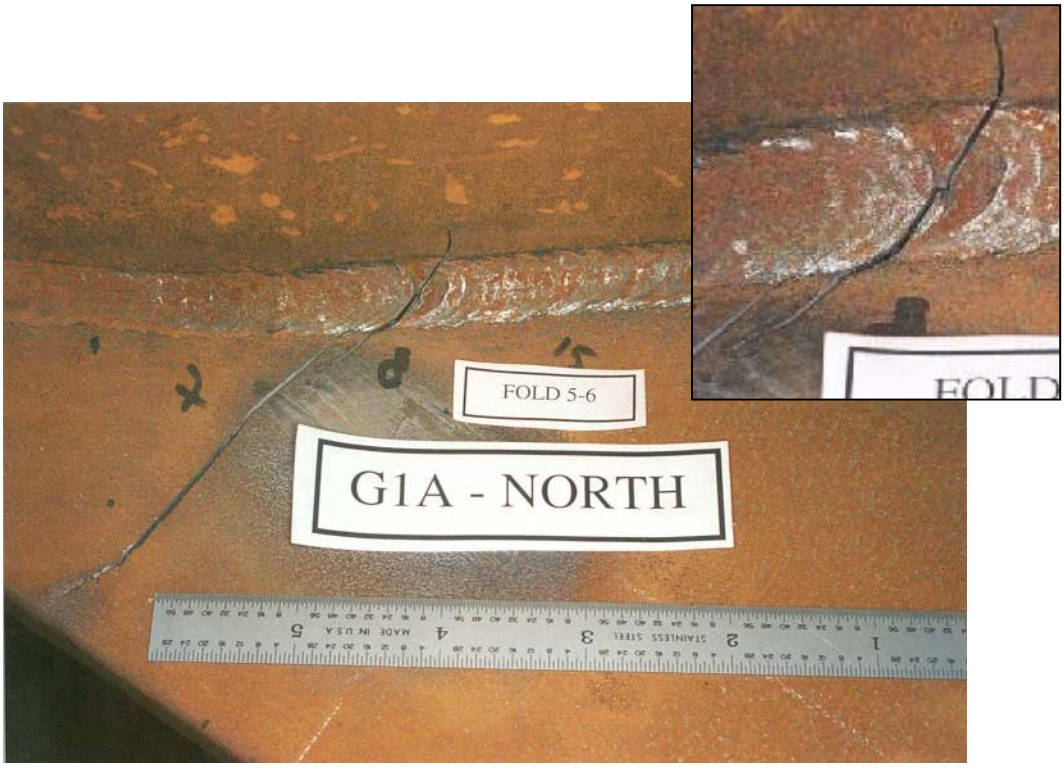

Figure 18. Main fatigue crack of Girder G1A.

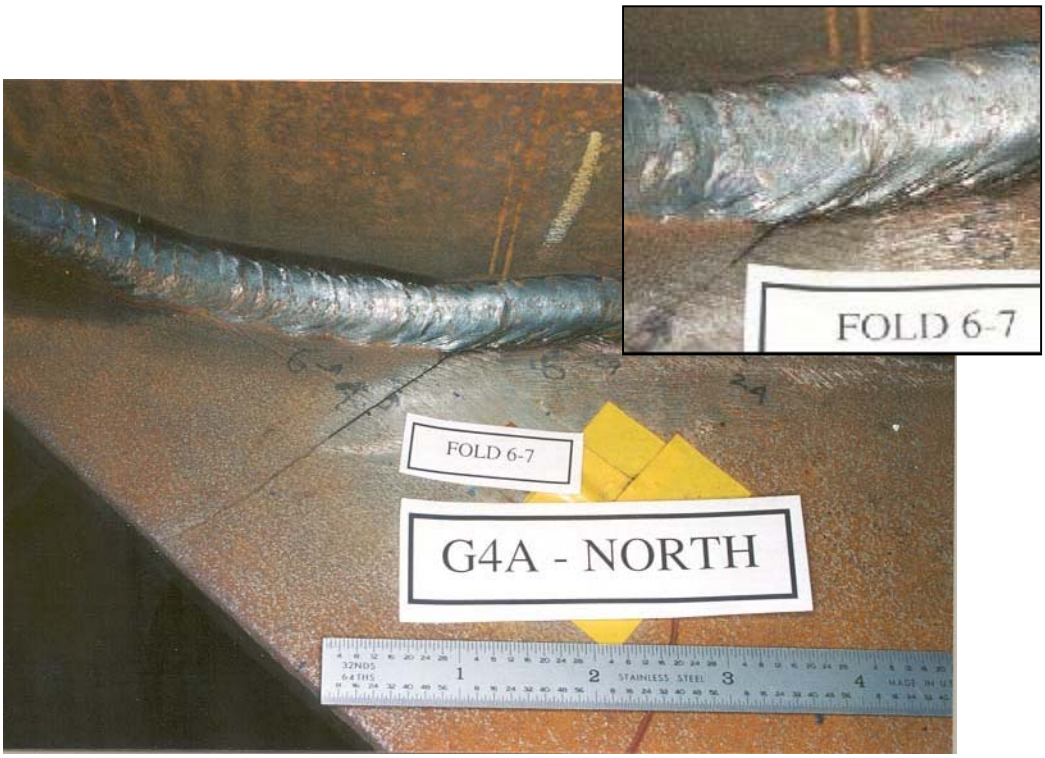

Figure 19. Main fatigue crack of Girder G4A.

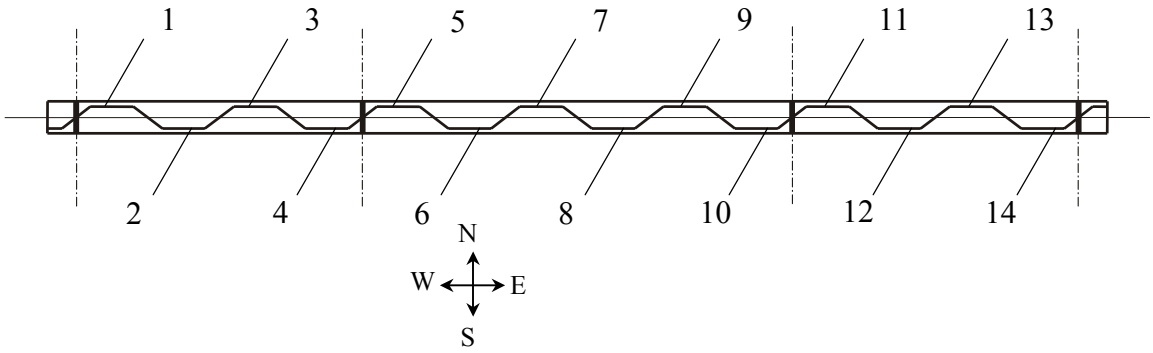

Figure 20. Numbering scheme for longitudinal web folds.

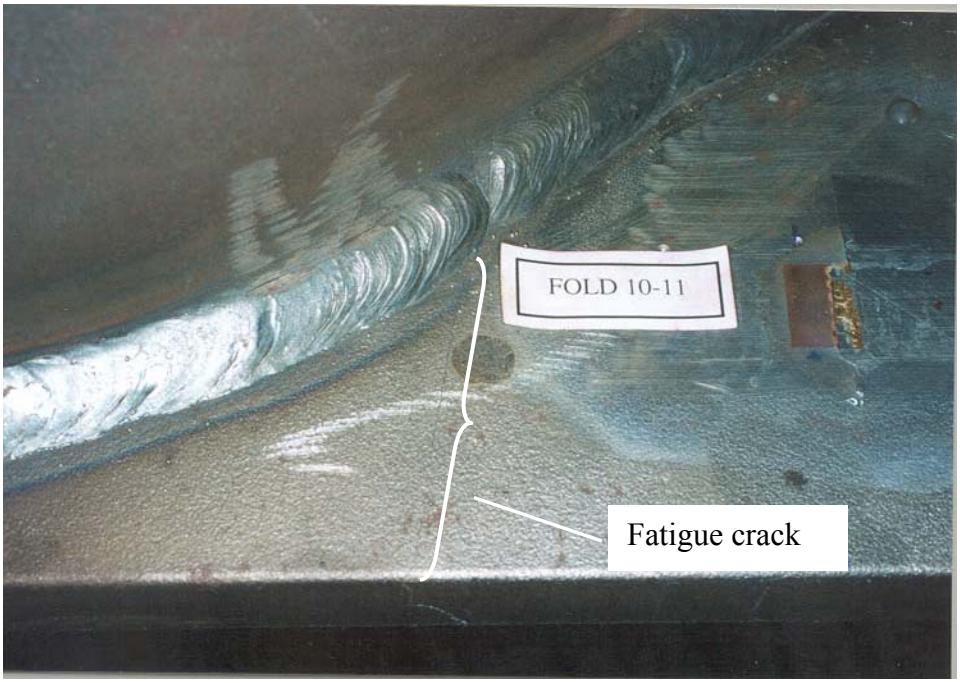

Figure 21. Main fatigue crack of Girder G6A.

(a) North side

(b) South side

Figure 22. Variable quality of welds of Girder G6A.

Figure 23. Failure of Girder G4B.

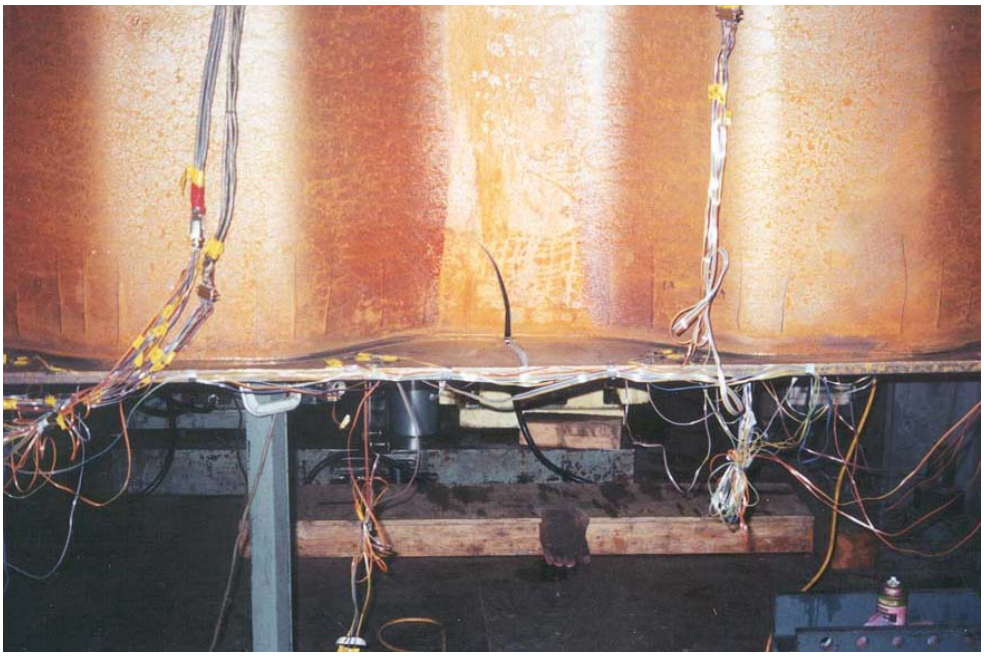

Figure 24. Failure of Girder G1B.

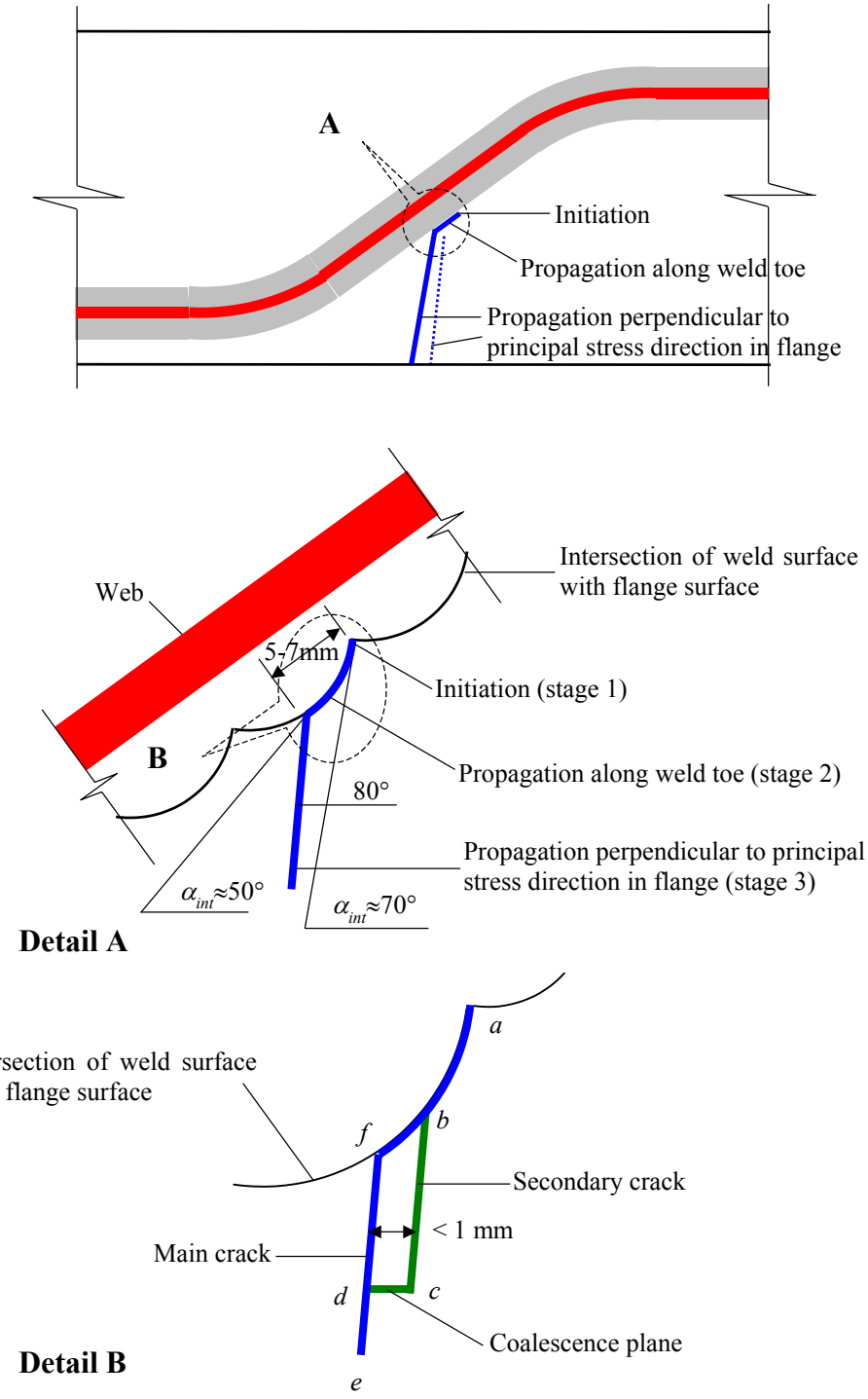

Figure 25. Observed crack patterns for semiautomatic GMAW process welds.

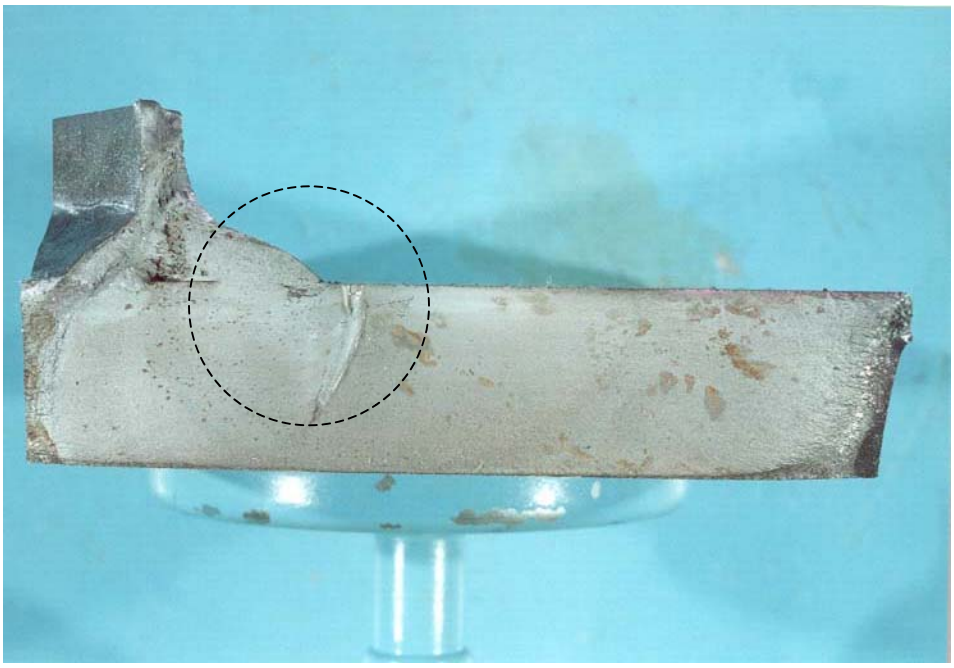

(a) Overall

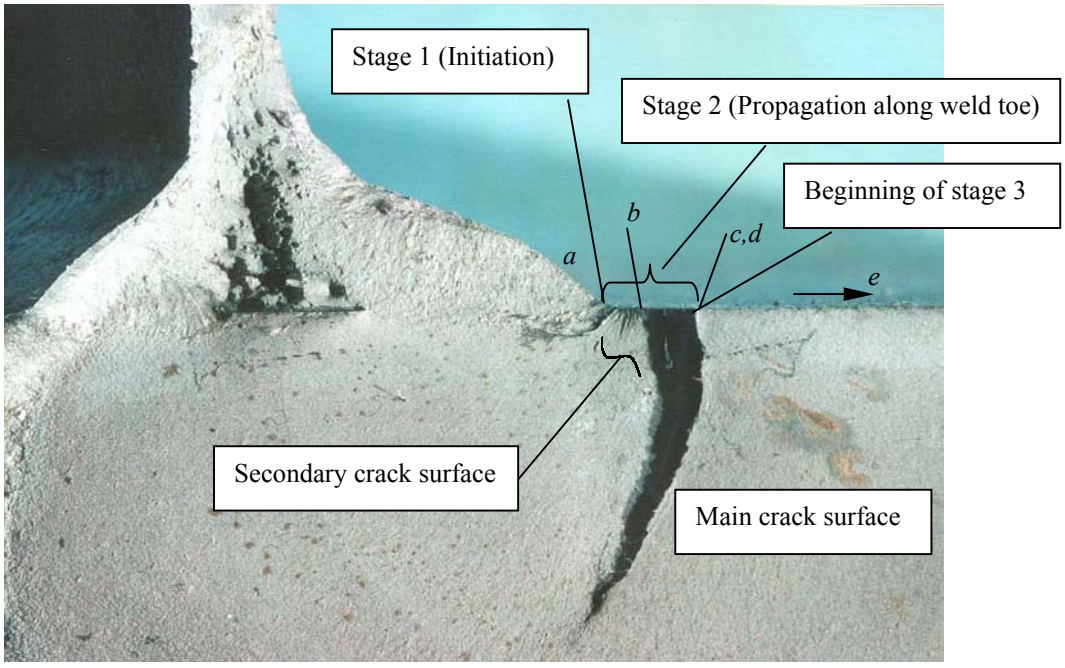

(b) Close-up

Figure 26. Fracture surface from Girder G2A.

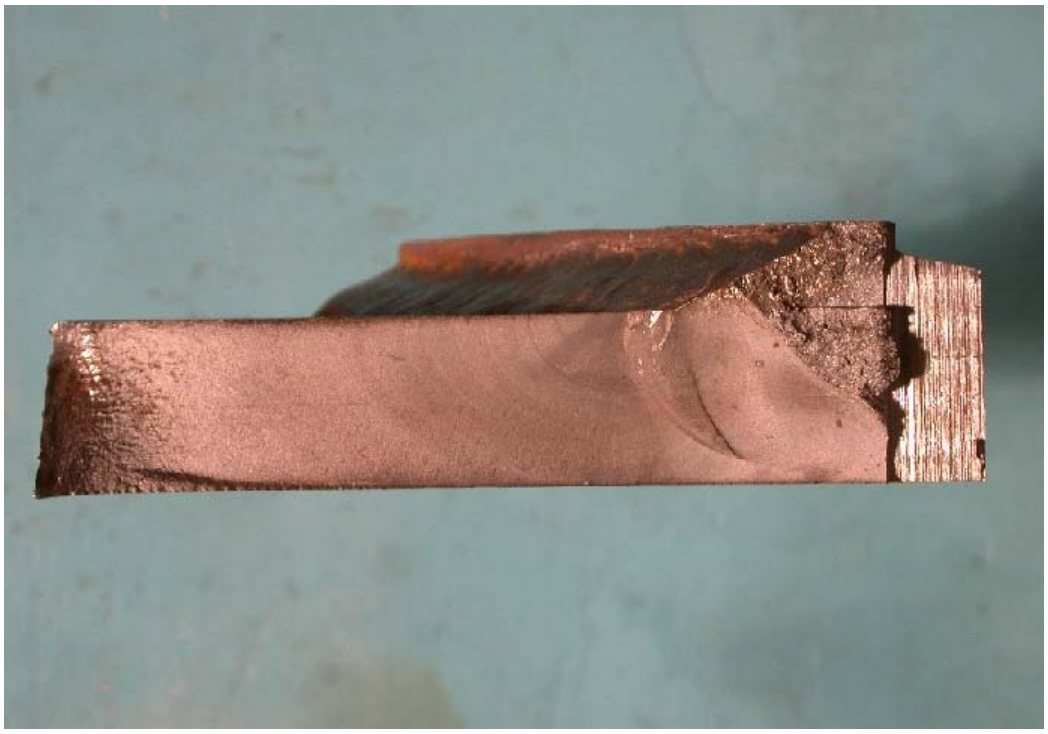

Figure 27. Fracture surface from Girder G4A.

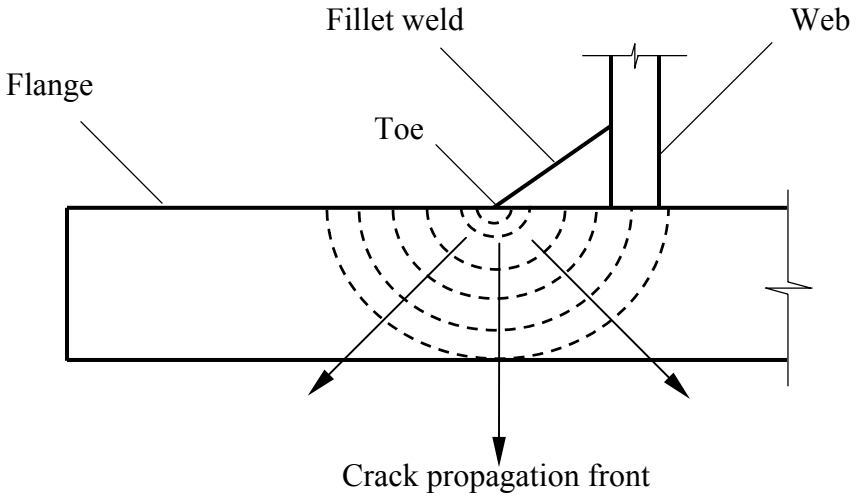

Figure 28. Idealized semi-elliptic pattern of fatigue crack growth during stage 3.

5. Analysis of Test Results

5.1. Analysis Based on Nominal Stresses

Based on the nominal stresses, the test data from the current investigation are plotted in Figure 29 with the mean S-N curves for the AASHTO LRFD fatigue categories. The data obtained by Ibrahim (2001) are also plotted for comparison. The data from Ibrahim (2001) are particularly relevant because the angle of corrugation is the same for the two sets of girders. The test data generally fall in a band between the mean for Category B and the mean for Category C, as anticipated from the previous experimental results. It appears that the mean for Category B′ fits the data reasonably well. The robotically welded girders exhibited an increased fatigue life, but their data points are also below the mean for Category B.

The data are re-plotted in Figure 30 with the design S-N curves for the AASHTO LRFD fatigue categories. The data include all existing fatigue test results relevant to corrugated web bridge girders. Although the majority of data from previous research are above the Category B design curve, the data from the current study are often below Category B. The fatigue resistance of Category B′ provides a reasonable lower bound to the test results.

5.2. Remaining Fatigue Life Analysis

The eight fatigue tests of the current investigation produced (directly) eight fatigue life data points for corrugated web I-girders. The analysis described in this section takes advantage of the multiple fatigue cracks observed during the tests to increase the number of data points available from these tests. The test results show that multiple fatigue cracks initiated at the web-to-flange fillet weld toe along the inclined web folds within the constant moment region. The tests were terminated when the most critical crack propagated through the flange thickness and to the flange tip. Here, test data for other less critical fatigue cracks are used to estimate additional fatigue life data.

Where possible, the remaining fatigue life (the number of cycles to failure N_r) of the largest partially propagated crack along each inclined web fold was estimated and added to the accumulated life at the end of the physical test (the accumulated number of cycles) to determine the total life for each of these cracks.

The fracture surface studies suggested that, during the final propagation stage (stage 3), the fatigue cracks could be assumed semi-elliptical in shape, with the ratio of the minor semi-axis of the ellipse, a, to the major semi-axis of the ellipse, c, equal to 0.75. Figure 31 shows the assumptions used to calculate the remaining life, N_r. In Figure 31, the dimension a_i is the initial crack depth, and a_i is estimated as $0.75c_i$ where c_i is the observed initial crack length. a_f is the final crack depth, which is the flange thickness, t_f, because, after the crack propagates through the flange plate thickness, the remaining

number of cycles needed to propagate the crack to the flange tip is small and can be neglected.

N_r is estimated from a crack propagation analysis. The fatigue crack propagation per cycle, *da/dN*, is related to the stress intensity factor range, ΔK, as follows (Paris 1962, Paris and Erdogan 1963):

$$\frac{da}{dN} = C(\Delta K)^n \tag{6}$$

where, a is the crack size, N is the number of cycles, and C and n are material constants. By integrating Equation 6, the number of cycles, N, required to propagate a crack from an initial size a_i to a final size a_f can be determined:

$$N = \frac{1}{C}\int_{a_i}^{a_f} \frac{da}{\Delta K^n} \tag{7}$$

ΔK, the stress intensity factor range in Equations 6 and 7, is analogous to the stress intensity factor, K. Linear elastic fracture mechanics can be used to establish ΔK as summarized briefly below.

At the tip of a central through-thickness crack of size $2a$ in an infinite plate subjected to a uniform tensile stress, σ, the stress intensity factor, K, is given by (Irwin 1961):

$$K = \sigma\sqrt{\pi\ a} \tag{8}$$

For other crack conditions, Albrecht and Yamada (1977) proposed the following:

$$K = F(a)\sigma\sqrt{\pi\ a} \tag{9}$$

where *F(a)* represents a crack size dependent correction factor for conditions other than an infinite plate with a central through-thickness crack, and is given by:

$$F(a) = F_E\, F_S\, F_W\, F_G \tag{10}$$

where, F_E is the crack shape correction factor, F_S is the front free surface correction factor, F_W is the finite plate width correction factor, and F_G is the stress gradient correction factor.

For an elliptical crack in an infinite solid subjected to uniform tension, F_E is given by:

$$F_E = \frac{1}{E_k} \tag{11}$$

where, E_k is an elliptical integral of the second kind, given by:

$$E_k = \int_0^{\pi/2} \left[1 - \left(1 - \frac{a^2}{c^2} \right) \sin^2 \varphi \right]^{1/2} d\varphi \tag{12}$$

in which φ is an integration parameter. For a semi-elliptic edge crack, various researchers (*e.g.,* Tada *et al*. 2000) suggest the following for F_S:

$$F_S = 1 + 0.12 \left(1 - \frac{a}{c} \right) \tag{13}$$

Equation 13 suggests that for long shallow cracks (*i.e.,* when $a<<c$), F_S will approach the theoretical value of 1.12 for an edge crack in a semi-infinite plate, whereas for semicircular cracks (*i.e.,* when $a=c$), F_S will equal 1.

For a plate with finite width and a central through-thickness crack of size $2a$ subjected to a uniform tensile stress, σ, Paris and Sih (1964) proposed the following stress intensity factor:

$$K = \sqrt{\frac{W}{\pi\ a} \tan\left(\frac{\pi\ a}{W} \right)} \sigma \sqrt{\pi\ a} \tag{14}$$

where, W is the plate width. From Equation 14, which is considered accurate for $2a/W$ ratios up to ½, F_W is as follows:

$$F_W = \sqrt{\frac{W}{\pi\ a} \tan\left(\frac{\pi\ a}{W} \right)} \tag{15}$$

F_G accounts for the effect of local stress concentration. Fatigue cracks initiate at geometric discontinuities where cover plates, transverse stiffeners, and so on, are attached to flange and web plates. Immediately adjacent to the attachment is an area of high stress concentration. As the cracks grow into the plate, they grow away from the area of high stress concentration. Accurately knowing F_G is important for situations where the calculated fatigue life includes fatigue crack propagation in the region of high stress concentration. The largest cracks on the inclined folds of the fatigue test girders were partially propagated into the flange plate, so for determining the remaining life of these cracks, it is reasonable to assume that F_G is 1.

The remaining life, N_r, was estimated using Equation 7. From Equations 9 and 10, the stress intensity factor range, ΔK was calculated as follows:

$$\Delta K = F_E\ F_S\ F_W\ F_G \Delta\sigma \sqrt{\pi\ a} \tag{16}$$

where:

$$F_E = 1.38$$
$$F_S = 1.03$$
$$F_W = \sqrt{\frac{2t_f}{\pi\ a}\tan\left(\frac{\pi\ a}{2t_f}\right)} \quad (17)$$
$$F_G = 1$$

The numerical values of F_E and F_S, were computed using Equations 11 and 13, respectively. The expression for F_W is Equation 15 with W replaced by $2t_f$. Additionally, the constant C is equal to 9.69×10^{-4} mm$^{5.5}$/kN^2 (3.6×10^{-10} in$^{5.5}$/kip^2) and constant n is equal to 3, as proposed by Barsom and Rolfe (1999) for ferrite-pearlite steels. These values were selected because they provided good correlation between the experimental results and the remaining life analysis. The longitudinal stress range, $\Delta\sigma$, in front of the crack was estimated from strain gage measurements.

The largest flange crack (propagating from the web-to-flange fillet weld) along each inclined web fold was identified and its dimension c_i (used to estimate a_i for Equation 7) as well as its distance to the flange edge were measured. The results are summarized in Table 5. The remaining fatigue life analysis considered only the flange regions along inclined web folds where cracks were detected and flange strain measurements were available. Table 5 compares the measured longitudinal stress ranges to the nominal stress ranges in these flange regions. The comparison shows that the measured stresses in front of the crack location on the top surface of the bottom (tension) flange are always higher than the nominal stresses.

The total fatigue life for the largest crack along each inclined fold, N_t, is estimated as:

$$N_t = N + N_r \quad (18)$$

where, N is the accumulated number of cycles at the end of the test. The results are summarized in Table 6. A graphical representation of the data of Table 6 is plotted in Figure 32 with the mean S-N curves for the AASHTO LRFD fatigue categories. The best fit equation for the data from the remaining life analysis (with a slope of –3) is given by:

$$log\ N = 12.6758 - 3\,log\,\sigma_r \quad (19)$$

In deriving Equation 19, the data corresponding to fatigue cracks that were located beyond the ends of the flat portion of an inclined fold were discarded, because the estimated stress in front of the crack location is considered reliable for locations where the inclined fold is flat, but not reliable for the bend region. Table 1 shows that the constant of Equation 19, *log A* equal to 12.6758, clearly falls between *log A* for the mean S-N curve for Category B and *log A* for the mean S-N curve for Category C, and extremely close to *log A* for the mean S-N curve for Category B′.

5.3. Fatigue Design Criteria

The results of the fatigue tests are considered applicable to corrugated web girders with the corrugated web geometries similar to that shown in Figure 7. For finite life fatigue design calculations, the design S-N curve for Category B′ of the AASHTO LRFD fatigue specifications is recommended. Comparison of the test results with the mean S-N curves shows that the data fit the mean for Category B′ reasonably well.

For the constant amplitude fatigue limit (CAFL), a value of 96.5 MPa (14 ksi), which lies between the CAFL of Category B and Category C, is recommended for fatigue design calculations. This gives an improvement in fatigue strength of 40% and 17% over Category C and Category B′/C′, respectively. The design recommendations are shown in Figure 33.

The design stress range should be calculated considering flange transverse bending moments that develop due to shear forces in corrugated web girders. The longitudinal stresses in the flange, σ, can be determined by superposition:

$$\sigma = \frac{M_x Y}{I_x} + \frac{M_t x}{I_t} \tag{20}$$

where, M_x and M_t are the overall bending moment and the flange transverse bending moment, respectively, I_x and I_t are the moment of inertia of the girder cross section and the transverse bending moment of inertia of the flange, respectively, Y is the distance from the neutral axis of the cross section to the point under investigation, and x is the distance from the centerline of the flange to the point under investigation. M_t is discussed in detail by Abbas (2003), and briefly by Sause *et al*. (2003). The maximum value of x used in Equation 20 need not exceed one half of the web corrugation depth, but should not be less than the distance from the flange centerline to the end of the flat portion of the inclined web fold.

Table 5. Crack information used in remaining fatigue life analysis.

Girder/Fold	Measured Stress Range (MPa)	Ratio of Measured to Nominal Stress Range	c_i (mm)	a_i (mm)	Edge Distance (mm)
G2A/7-8	146	1.06	11.1	8.3	111.1
G1A/4-5	150.	1.09	4.8	3.6	67.5
G1A/5-6	155	1.12	--	--	75.0
G1A/6-7	146	1.06	7.9	5.9	81.0
G1A/7-8	148	1.07	9.5	7.1	91.3
G1A/8-9	145	1.05	9.5	7.1	126.2
G1A/9-01	142	1.03	10.3	7.7	85.7
G1A/10-11	140.	1.01	11.1	8.3	71.4
G4A/4-5	147	1.07	3.2	2.4	73.0
G4A/5-6	146	1.06	8.7	6.5	98.4
G4A/6-7	153	1.11	--	--	69.0
G4A/7-8	149	1.08	6.4	4.8	93.7
G4A/8-9	152	1.10	19.8	14.9	96.0
G4A/9-10	**167**	**1.21**	**10.3**	**7.7**	**47.6**
G4A/10-11	**156**	**1.13**	**12.7**	**9.5**	**49.2**
G5A/9-10	120.	1.16	6.4	4.8	66.0
G6A/4-5	111	1.07	2.4	1.8	110.3
G6A/6-7	109	1.06	7.9	5.9	111.9
G6A/8-9	**120.**	**1.16**	**4.0**	**3.0**	**45.2**
G6A/10-11	126	1.21	--	--	53.0
G3A/8-9	110.	1.06	12.7	9.5	106.8

Note: Cracks with data in bold were not used in regression analysis

Table 6. Summary of remaining fatigue life analysis.

Girder/Fold	Measured Stress Range (MPa)	Remaining Life, N_r	Total Life, N_t
G2A/7-8	146	75,800	1,493,800
G1A/4-5	150.	262,200	1,710,200
G1A/5-6	155	0	1,448,000
G1A/6-7	146	144,700	1,592,700
G1A/7-8	148	101,300	1,549,300
G1A/8-9	145	108,900	1,556,900
G1A/9-01	142	98,000	1,546,000
G1A/10-11	140.	86,900	1,534,900
G4A/4-5	147	421,000	1,724,500
G4A/5-6	146	125,200	1,428,700
G4A/6-7	153	0	1,303,500
G4A/7-8	149	188,400	1,491,900
G4A/8-9	152	7000	1,310,500
G4A/9-10	**167**	**60,000**	**1,363,500**
G4A/10-11	**156**	**44,800**	**1,348,300**
G5A/9-10	120.	361,200	2,353,400
G6A/4-5	111	1,264,500	3,827,900
G6A/6-7	109	346,900	2,910,300
G6A/8-9	**120.**	**619,200**	**3,182,600**
G6A/10-11	126	0	2,563,400
G3A/8-9	110.	128,100	3,564,200

Note: Cracks with data in bold were not used in regression analysis

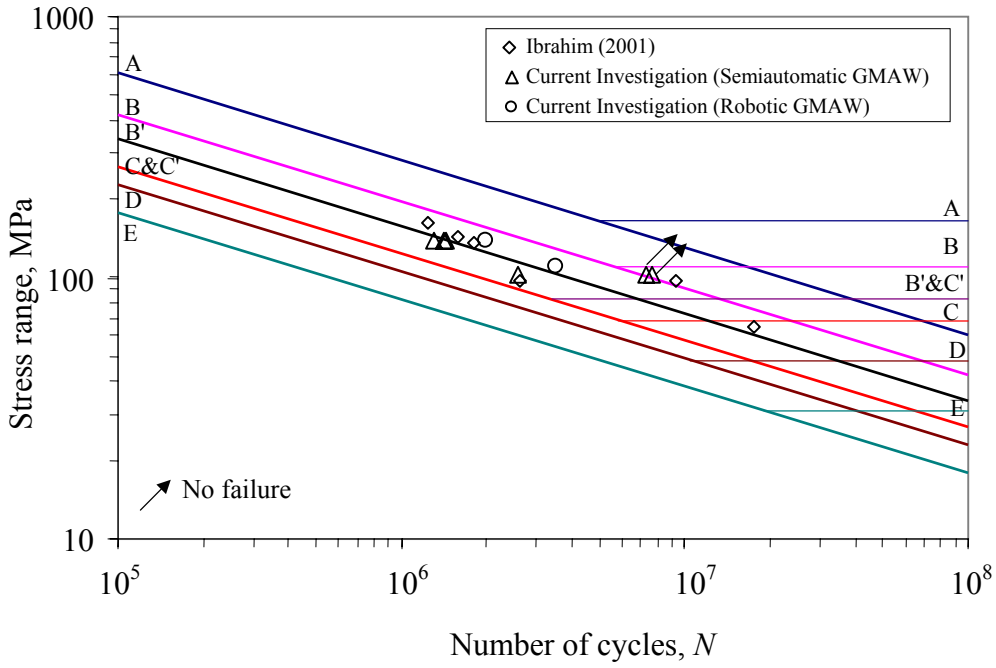

Figure 29. Fatigue test data for corrugated web girders (with trapezoidal corrugations) with mean S-N curves for AASHTO LRFD fatigue categories.

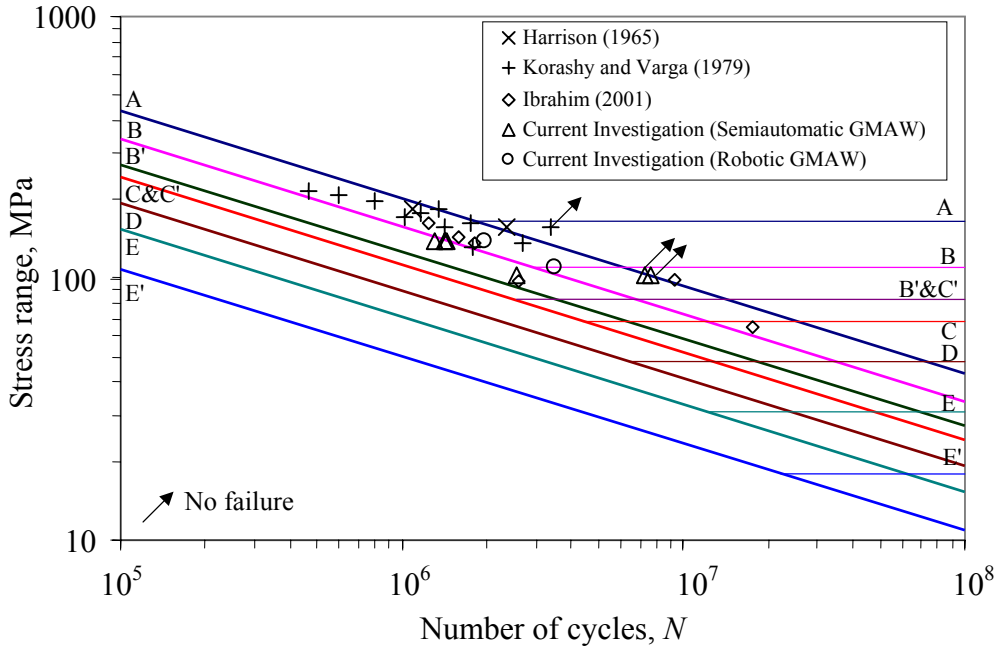

Figure 30. Fatigue test data for corrugated web girders with design S-N curves for AASHTO LRFD fatigue categories.

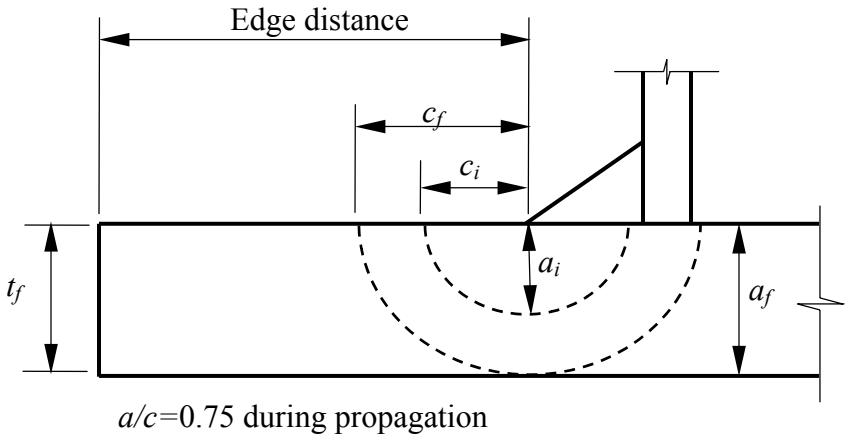

Figure 31. Remaining life analysis assumptions.

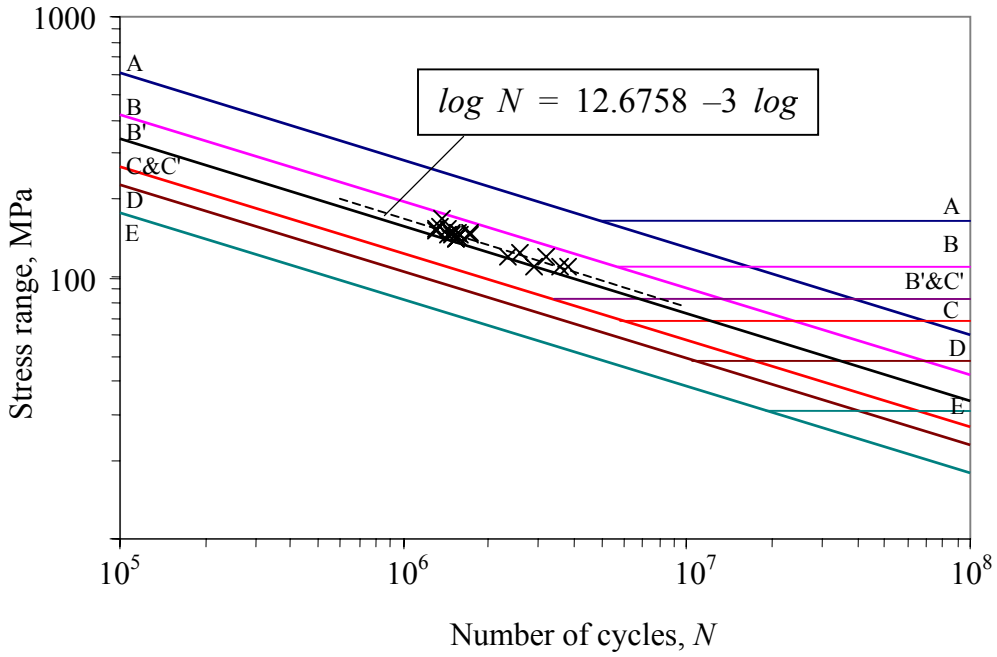

Figure 32. Analytically determined fatigue data with mean S-N curves for AASHTO LRFD fatigue categories.

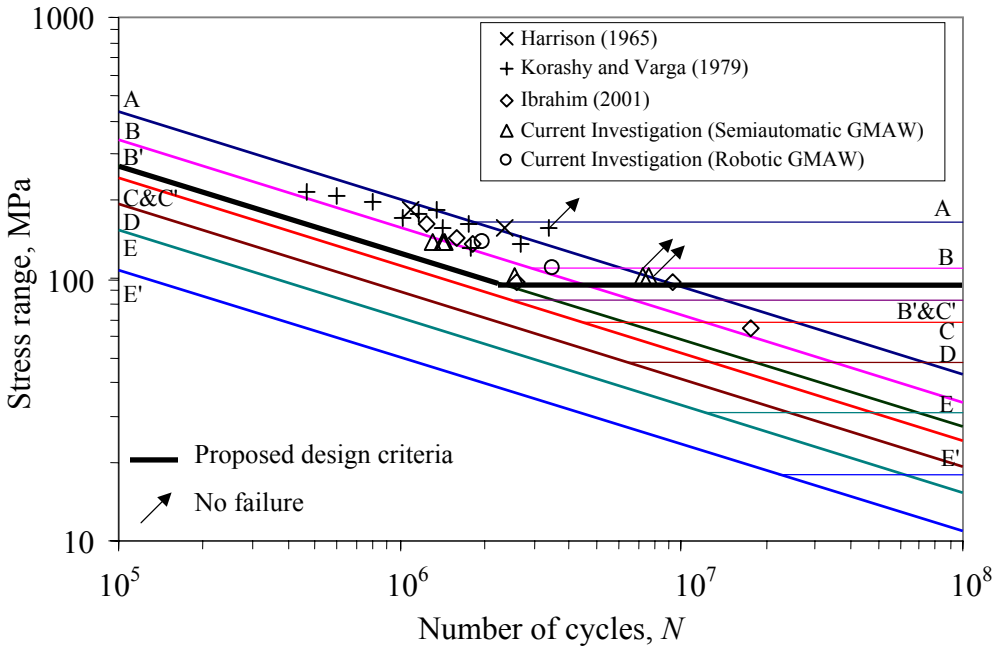

Figure 33. Design recommendations for corrugated web I-girders.

6. Summary and Conclusions

This report provides data on the fatigue strength and proposes fatigue design criteria for corrugated web I-girders for bridges with trapezoidal corrugations. Eight large-scale test specimens, representative of bridge girders, were designed, fabricated, and tested, resulting in eight fatigue life versus stress range data points.

The test specimens were made of ASTM A709 HPS-485W (HPS-70W) steel (ASTM 2001), and were tested in 4-point bending. The web-to-flange fillet welds were made using semiautomatic gas metal arc welding (GMAW) for Girders G1A to G6A, and robotic GMAW for Girders G1B and G4B. Visual inspection showed that robotic welding produced quality fillet welds with a remarkably uniform weld toe geometry, compared to the semiautomatic GMAW process.

The test girders that failed in fatigue failed from cracks that initiated and propagated in the bottom (tension) flange within the constant moment test region of the girders. Some test girders did not develop detectable cracks within the test region. The fatigue life of the robotically welded Girder G4B, tested at a nominal stress range of 138 MPa (20.0 ksi), was approximately 42% higher than the fatigue life of similar girders welded using semiautomatic GMAW.

Fatigue cracks generally initiated at the web-to-flange fillet weld toe along the inclined web folds and the bend regions adjacent to the inclined folds. For the girders welded using semiautomatic GMAW, the point of fatigue crack initiation was almost always where the surfaces of two weld ripples intersect with the flange surface. The initial stage of crack propagation was along the weld toe. The extent of this initial stage of crack propagation depended on the local geometry at the weld toe. In the final stage of propagation the cracks turned into the flange and propagated perpendicular to the principal stress direction and eventually to the flange tip causing the tests to be terminated.

In some of the test girders, many similar fatigue cracks were observed in the flange along the inclined web folds. Some of these multiple cracks were used in a remaining fatigue life analysis that resulted in 21 additional total fatigue life versus stress range data points.

The results of the current study, as well as previous research, demonstrate that girders with corrugated webs exhibit a fatigue life that is generally longer than conventional girders with transverse stiffeners (Category C) but shorter than unstiffened girders with flat webs (Category B). For the fatigue design of corrugated web girders, the Category B′ design curve of the AASHTO LRFD specifications (AASHTO 1998) is recommended for finite life fatigue design calculations, and a value of 96.5 MPa (14 ksi) for the constant amplitude fatigue limit (CAFL). This CAFL gives an improvement in fatigue strength of 40% and 17% over the CAFL of Category C and Category B′/C′, respectively.

References

AASHTO (1998) *AASHTO LRFD Bridge Design Specifications*, 2nd edition, American Association of State Highway and Transportation Officials, Washington, D.C., 1998.

Abbas, H.H. (2003) "Analysis and Design of Corrugated Web I-Girders for Bridges Using High Performance Steel, " Ph.D. Dissertation, Lehigh University, Bethlehem, PA.

Albrecht, P. and Yamada, K. (1977) "Rapid Calculation of Stress Intensity Factors," *Journal of the Structural Division*, Proceedings of the ASCE, Vol. 103, ST 2, pp. 377-389, February, 1977.

ASTM (2001) "A709/A709M-00a, Standard Specification for Carbon and High-Strength Low-Alloy Structural Steel Shapes, Plates, and Bars and Quenched-and-Tempered Alloy Structural Steel Plates for Bridges," *ASTM Annual Book of Standards, Vol. 01.04*, American Society for Testing and Materials, West Conshohocken, PA.

Barsom, J.W. and Rolfe, S.T. (1999) *Fracture and Fatigue Control in Strucutres*, 3rd Edition, American Society for Testing and Materials, West Conshohocken, PA.

Elgaaly, M., Seshadri, A., Rodriquez, R., and Ibrahim, S. (2000) "Bridge Girders with Corrugated Webs," Fifth International Bridge Engineering Conference, *Transportation Research Record 1696*, Paper No. 5B0022, pp. 162-170.

Fisher, J.W., Frank, K.H., Hirt, M.A., and McNamee, B.M. (1970) "Effect of Weldments on the Fatigue Strength of Steel Beams," NCHRP Report 102, Highway Research Board, Washington, D.C.

Fisher, J.W., Albrecht, P.A., Yen, B.T., Klingerman, D.J., and McNamee, B.M. (1974) "Fatigue Strength of Steel Beams with Welded Stiffeners and Attachments," NCHRP Report 147, Transportation Research Board, Washington, D.C.

Harrison, J.D. (1965) "Exploratory Fatigue Test of Two Girders with Corrugated Webs," *British Welding Journal*, pp. 121-125, March.

Ibrahim, S.A. (2001) "Fatigue Analysis and Instability Problems of Plate Girders with Corrugated Webs," Ph.D. Dissertation, Department of Civil and Architectural Engineering, Drexel University, Philadelphia, PA.

Irwin, G.R. (1961) "Fracturing and Fracture Mechanics," Theoretical and Applied Mechanics Reports 202, University of Illinois, Urbana, IL, October.

Kaufmann, E.J., Metrovich, B., Pense, A.W. (2001) "Characterization of Cyclic Inelastic Strain Behavior on Properties of A572 Gr. 50 and A913 Gr. 50 Rolled Sections," Report No. 01-13, Center for Advanced Technology for Large Structural Systems, Lehigh University, Bethlehem, PA, August.

Keating, P.B. and Fisher, J.W. (1986) "Evaluation of Fatigue Tests and Design Criteria on Welded Details," NCHRP Report 286, Transportation Research Board, Washington, D.C., September.

Korashy, M. and Varga, J. (1979) "Comparative Investigation of Fatigue Strength of Beams with Web Plate Stiffened in the Traditional Way and by Corrugation," *Acta Technica Academiae Scientiarum Hungaricae*, Vol. 89, No. 3-4, pp. 309-346.

Lindner, J. and Huang, B. (1995) "Beulwerte für Trapezförmig Profilierte Bleche unter Schubbeanspruchung," *Stahlbau*, Vol. 64, No. 12, pp. 370-374.

Paris, P.C. (1962) "The Growth of Fatigue Cracks due to Variations in Load," Ph.D. Dissertation, Lehigh University, Bethlehem, PA.

Paris, P.C. and Erdogan, F. (1963) "A Critical Analysis of Crack Propagation Laws," *Journal of Basic Engineering*, Transactions of the ASME, Series D, Vol. 85, pp. 528-534, December.

Paris, P.C. and Sih, G.C. (1964) "Stress Analysis of Cracks," ASTM Special Technical Publication, No. 381, American Society for Testing and Materials, pp. 30-81.

Rodriguez, R. (2000) "Stress Distribution and Bearing Stiffeners Details Related to Fatigue and Fracture of Steel Girders with Corrugated Webs," Ph.D. Dissertation, Department of Civil and Architectural Engineering, Drexel University, Philadelphia, PA.

Sause, R., Abbas, H.H., Wassef, W., Driver, R.G., and Elgaaly, M. (2003) "Corrugated Web Girder Shape and Strength Criteria: Work Area 1, Pennsylvania Innovative High Performance Steel Bridge Demonstration Project," ATLSS Report No. 03-18, Center for Advanced Technology for Large Structural Systems, Lehigh University, Bethlehem, PA, September.

Sause, R. (2003) "Corrugated Web Girder Fabrication: Work Area 2, Pennsylvania Innovative High Performance Steel Bridge Demonstration Project," ATLSS Report No. 03-19, Center for Advanced Technology for Large Structural Systems, Lehigh University, Bethlehem, PA, August.

Statnikov, E.S. (1997) "Applications of Operational Ultrasonic Impact Treatment (UIT) Technologies in Production of Welded Joints," IIW/IIS Doc. XIII-1667-97, International Institute of Welding and International Iron and Steel Institute.

Tada, W., Paris, P.C., Irwin, G.R. (2000) *The Stress Analysis of Cracks Handbook*, 3rd Edition, American Society of Mechanical Engineers, New York, N.Y.

Takamori, H. and Fisher, J.W. (2000), "Tests of Large Girders Treated to Enhance Fatigue Strength," Fifth International Bridge Engineering Conference, *Transportation Research Record 1696*, Paper No. 5B0093, pp. 93-99.